

Predicting Drug Interactions with Human Equilibrative Nucleoside Transporters 1 and 2 Using Functional Knockout Cell Lines and Bayesian Modeling^{SI}

Siennah R. Miller, Xiaohong Zhang, Raymond K. Hau, Joseph L. Jilek, Erin Q. Jennings, James J. Galligan, Daniel H. Foil, Kimberley M. Zorn, Sean Ekins, Stephen H. Wright, and Nathan J. Cherrington

Department of Pharmacology and Toxicology, College of Pharmacy (S.R.M., R.K.H., J.L.J., E.Q.J., J.J.G., N.J.C.), and Department of Physiology, College of Medicine (X.Z., S.H.W.), University of Arizona, Tucson, Arizona and Collaborations Pharmaceuticals, Inc., Raleigh, North Carolina (D.H.F., K.M.Z., S.E.)

Received September 21, 2020; accepted November 19, 2020

ABSTRACT

Equilibrative nucleoside transporters (ENTs) 1 and 2 facilitate nucleoside transport across the blood-testis barrier (BTB). Improving drug entry into the testes with drugs that use endogenous transport pathways may lead to more effective treatments for diseases within the reproductive tract. In this study, CRISPR/CRISPR-associated protein 9 was used to generate HeLa cell lines in which ENT expression was limited to ENT1 or ENT2. We characterized uridine transport in these cell lines and generated Bayesian models to predict interactions with the ENTs. Quantification of [³H]uridine uptake in the presence of the ENT-specific inhibitor S-(4-nitrobenzyl)-6-thioinosine (NBMPR) demonstrated functional loss of each transporter. Nine nucleoside reverse-transcriptase inhibitors and 37 nucleoside/heterocycle analogs were evaluated to identify ENT interactions. Twenty-one compounds inhibited uridine uptake and abacavir, nevirapine, tica-grelor, and uridine triacetate had different IC₅₀ values for ENT1 and ENT2. Total accumulation of four identified inhibitors was measured with and without NBMPR to determine whether there was ENT-mediated transport. Clofarabine and cladribine were ENT1 and ENT2 substrates, whereas nevirapine and lexibulin were ENT1 and ENT2 nontransported inhibitors. Bayesian models generated

using Assay Central machine learning software yielded reasonably high internal validation performance (receiver operator characteristic > 0.7). ENT1 IC₅₀-based models were generated from ChEMBL; subvalidations using this training data set correctly predicted 58% of inhibitors when analyzing activity by percent uptake and 63% when using estimated-IC₅₀ values. Determining drug interactions with these transporters can be useful in identifying and predicting compounds that are ENT1 and ENT2 substrates and can thereby circumvent the BTB through this transepithelial transport pathway in Sertoli cells.

SIGNIFICANCE STATEMENT

This study is the first to predict drug interactions with equilibrative nucleoside transporter (ENT) 1 and ENT2 using Bayesian modeling. Novel CRISPR/CRISPR-associated protein 9 functional knockouts of ENT1 and ENT2 in HeLa S3 cells were generated and characterized. Determining drug interactions with these transporters can be useful in identifying and predicting compounds that are ENT1 and ENT2 substrates and can circumvent the blood-testis barrier through this transepithelial transport pathway in Sertoli cells.

Introduction

There is a need to understand and clarify the interactions between the equilibrative nucleoside transporters (ENTs) and nucleoside analogs. These ubiquitously expressed transporters play a role in the pharmacokinetics and drug-drug

interactions (DDIs) of nucleoside analogs, which share a similar chemical structure with endogenous substrates of these transporters (<http://www.proteinatlas.org>; Huber-Ruano and Pastor-Anglada, 2009; Koczor et al., 2012; Pastor-Anglada and Pérez-Torras, 2015; Rehan et al., 2019). Although there is clear value in heterologous expression systems to study the ENTs, the resulting models can be complicated to interpret; the complexity is caused by a variety of issues, including the influence of endogenous nucleoside transport activity (Ward et al., 2000; Sundaram et al., 2001; Yao et al., 2001; Boswell-Casteel and Hays, 2017). The disparity of published results using heterologous models highlights the value of experimental

This work was supported by National Institutes of Health National Institute of General Medical Sciences [Grant R01-GM123643], [Grant 1R-41GM131433-01A1] and [Grant R44-GM122196-02A1]; and National Institute of Environmental Health Sciences [Grants 5-P30-ES006694 and 2-T32-ES007091-36A1].
<https://doi.org/10.1124/molpharm.120.000169>

^{SI} This article has supplemental material available at molpharm.aspetjournals.org.

ABBREVIATIONS: ACN, acetonitrile; BTB, blood-testis barrier; Cas9, CRISPR-associated protein 9; DDI, drug-drug interaction; ENT, equilibrative nucleoside transporter; GAPDH, glyceraldehyde-3-phosphate dehydrogenase; GC, guanine-cytosine; gRNA, guide RNA; KO, knockout; LC-MS/MS, liquid chromatography tandem mass spectrometry; LyB, lysogeny broth; MCC, Matthews correlation coefficient; MGT, male genital tract; NBMPR, S-[(4-nitrophenyl)methyl]-6-thioinosine; NRTI, nucleoside reverse-transcriptase inhibitor; PCR, polymerase chain reaction; ROC, receiver operator characteristic; WB, Waymouth's buffer.

systems with natively expressed ENTs, which have more consistent results in the literature (Lauzon and Paterson, 1977; Plagemann et al., 1978; Dahlig-Harley et al., 1981; Griffith and Jarvis, 1996; Boleti et al., 1997; Mackey et al., 1999; Ward et al., 2000; Miller et al., 2020). Recent work has pharmacologically separated native ENT1 and ENT2 activity in wild-type HeLa S3 cells with the ENT inhibitor 6-S-[(4-nitrophenyl)methyl]-6-thioinosine (NBMPR) (Miller et al., 2020), but there is need for a more efficient, high-throughput method of studying the interactions between individual ENTs and nucleoside analogs.

Nucleoside analogs are used to treat health conditions, including viral infections and cancers, by interfering with nucleic acid synthesis (Ewald et al., 2008; Jordheim et al., 2013). These include the nucleoside reverse-transcriptase inhibitors (NRTIs) and DNA or RNA polymerase inhibitors used to treat various cancers, human immunodeficiency virus, and respiratory viruses (Ewald et al., 2008; Jordheim et al., 2013; Lucas and Nelson, 2015; Jordan et al., 2018). Nucleoside analogs have a long history of success, and this class of therapeutics recently gained attention with the emergency use of the nucleotide analog remdesivir to treat coronavirus disease 2019 (Eastman et al., 2020). Although there are many applications of nucleoside analogs, diseases that persist in sanctuary sites may be more difficult to treat because of the inability of compounds to reach effective concentrations. This includes the testis, where the blood-testis barrier (BTB) may prevent drugs from reaching therapeutically active concentrations within the male genital tract (MGT) (Le Tortorec and Dejucq-Rainsford, 2010; Durmus et al., 2015). The BTB protects developing germ cells from potentially harmful agents and can interfere with drug disposition to the MGT (Mruk and Cheng, 2015; Miller and Cherrington, 2018). Some viruses are sexually transmitted, and certain cancers negatively impact the structure and function of the MGT. SARS-CoV-2 viral loads are detectable in the semen of infected and recovering patients, indicating that it has the potential to be sexually transmitted (Cardona Maya et al., 2020; Li et al., 2020). Additionally, a clinical trial with Ebola virus survivors is investigating the potential of remdesivir to eradicate the virus from semen to prevent sexual transmission (National Institute of Allergy and Infectious Diseases, 2019). Therefore, it is essential that therapeutics reach effective concentrations in sanctuary sites to reduce viral transmission and/or eradicate the disease in question.

Transporters at the basal and apical membranes of testicular epithelial cells (Sertoli cells) provide a mechanism of bypassing the BTB (Mruk et al., 2011; Miller and Cherrington, 2018). ENT1 on the basal membrane and ENT2 on the apical membrane of Sertoli cells create a transepithelial transport pathway in which substrates of these transporters can enter the seminiferous lumen (Klein et al., 2013). Uridine is a well established substrate of both ENT1 and ENT2 and can be used to study the interaction of various nucleoside analogs on its transport (Ward et al., 2000; Kato et al., 2005; Klein et al., 2013; Miller et al., 2020).

The present study generated the first CRISPR/Cas9 functional knockouts of ENT1 and ENT2 from HeLa S3 cells natively expressing both transporters; the ENT2-knockout cells retained functional ENT1, and the ENT1-knockout cells retained functional ENT2. Interactions of endogenous nucleosides, NRTIs, and an additional set of nucleoside/heterocycle

analogues were studied to identify inhibitory interactions with ENT1 and ENT2. Additional transport studies were performed to determine whether four identified inhibitors of the ENTs enter cells through an ENT-mediated mechanism. Bayesian machine learning was used to identify structural elements found in effective inhibitors of ENT1- and ENT2-mediated transport. Predicting interactions with these transporters can aid the development of novel compounds that can cross the BTB using the ENT1-ENT2 transepithelial transport pathway. These include novel antivirals and chemotherapeutics that are substrates for these widely expressed transporters.

Materials and Methods

Reagents. Oligonucleotide primers were purchased from Integrated DNA Technologies (Coralville, IA). Lysogeny broth (LyB) and LyB agar plates with 50 µg/ml ampicillin and LyB were purchased through the University of Arizona BIO5 Media Facility. Moloney Murine Leukemia Virus Reverse Transcriptase (M-MLV RT), Platinum Taq DNA Polymerase High Fidelity, 10× BlueJuice gel loading buffer, UltraPure ethidium bromide, and the Invitrogen Cells-to-cDNA II Kit were purchased from Invitrogen (Carlsbad, CA). Phusion High-Fidelity Polymerase Chain Reaction (PCR) Mix with Guanidine Cytosine content Buffer was purchased from New England Biolabs (Ipswich, MA). Quantum Prep Freeze 'N Squeeze DNA Gel Extraction Spin Columns were purchased from BioRad (Hercules, CA). [³H] uridine (specific activity 35.2 Ci/mmol) was purchased from Perkin-Elmer (Waltham, MA). Uridine, adenosine, inosine, guanosine, cytidine, thymidine, and nevirapine were purchased from Sigma-Aldrich (St. Louis, MO). 6-NBMPR was purchased from Tocris (Bristol, UK). Abacavir sulfate, entecavir hydrate, zidovudine, didanosine, lamivudine, emtricitabine, tenofovir disoproxil, stavudine, zalcitabine, clofarabine, cladribine, and lexibulin were purchased from Cayman Chemical (Ann Arbor, MI). Thirty-seven nucleoside/heterocycle analogs were identified from the literature, selected, and provided as a generous gift from Gilead Sciences Inc. (Foster City, CA). Additional reagents were purchased from Thermo-Fisher Scientific unless otherwise noted.

Cell Culture. HeLa S3 CCL-2.2 cells were purchased from American Type Culture Collection and grown in Ham's F12K Media supplemented with 1.5 g/l sodium bicarbonate, 10% v/v FBS, and 1% v/v penicillin and streptomycin as previously described (Miller et al., 2020). Cells were propagated using the American Type Culture Collection protocol and kept at 37°C in a humidified 5% CO₂ incubator. Knockout HeLa S3 cell lines were cultured in the same conditions as wild-type HeLa S3 cells.

Generation of ENT1 and ENT2 HeLa Knockout Cell Lines. Guide RNA (gRNA) oligonucleotides for ENT1 and ENT2 were designed using the biology software Benchling (San Francisco, CA). The deletion for ENT1 was directed to be located in exon 5 with the gRNA forward sequence 5'-CACCGAGGTAGGTGAATAACAGCA-3' and the reverse sequence 5'-aaacTGCTGTTATTCACCTACCTC-3'. The deletion for ENT2 was directed to be located in exon 1 with the gRNA forward sequence 5'-CACCGTGGCGGAGGACGCCCCG-3' and the reverse sequence 5'-aaacCGGGCGTCTCCTCGCCAC-3'. The pSp-Cas9(BB)-2A-GFP (PX458) plasmid, a gift from Feng Zhang (Addgene, Watertown, MA) (Ran et al., 2013), was prepared with gRNA inserts for either ENT1 or ENT2 as described by Cong and Zhang (2015). The PX458 plasmid containing the gRNA inserts for either ENT1 or ENT2 was transformed into DH5α cells (New England Biolabs, Ipswich, MA). The transformed DH5α cells were then inoculated on LyB agar plates containing 50 µg/ml ampicillin and incubated at 37°C overnight. Single colonies were then inoculated into LyB supplemented with 100 µg/ml ampicillin and incubated at 37°C overnight in a shaker at 250 rpm. A QIAprep Spin Miniprep Kit

(Qiagen, Hilden, Germany) was used to purify the plasmid DNA according to the manufacturer's protocol. Concentration of the plasmid DNA was determined using a Spectrophotometer NanoDrop ND-1000 (Thermo-Fisher Scientific, Waltham, MA). The purified plasmids were sequenced with the primer: 5'-TTTATGGC-GAGGCGGCG-3' to confirm successful integration of the gRNA inserts.

Wild-type HeLa S3 cells were seeded 200,000 cells/well in a six-well plate 1 day prior to transfection. Cells were incubated with a mixture of 5 μ l of LipofectAMINE 3000, 1.25 μ l of P3000, and 1.2 μ g of plasmid DNA with gRNA inserts for ENT1 or ENT2 in 2 ml of Opti-minimum Eagle's medium per well for 24 hours at 37°C. Media were replaced 24 hours later, and cells were allowed to recover for 24 hours. Cells were passed and collected in preparation for fluorescence-assisted single-cell sorting using the BD FACSAria III at the Cytometry Core Facility at the University of Arizona. Data were analyzed using BD FACSDiva version 8.0.2. Single fluorescing cells were sorted into individual wells of two 96-well plates per cell line. Clones were maintained until a sufficient number of cells were obtained to assess successful knockout of either ENT1 or ENT2 (Cong and Zhang, 2015; Gaffney et al., 2020).

Polymerase Chain Reaction and Sanger Sequencing. The Invitrogen Cells-to-cDNA II Kit was used to generate cDNA from wild-type HeLa S3 cells, ENT1 KO cells, and ENT2 KO cells. Approximately 100,000 cells per cell line were harvested and prepared for reverse transcription. Briefly, 10 μ l of the lysate was incubated with 1 μ l of 10 mM deoxynucleotide triphosphate and 1 μ l of 18-mer oligo deoxythymine (dT) primers at 65°C for 5 minutes and briefly chilled on ice. Next, 4 μ l of 5 \times first-strand buffer, 2 μ l of 0.1 mM dithiothreitol, 1 μ l of Moloney Murine Leukemia Virus Reverse Transcriptase (M-MLV RT), and 1 μ l of RNase inhibitor were added (final volume 20 μ l) and incubated at 37°C for 50 minutes and then 70°C for 15 minutes.

For PCR amplification of ENT1, 3.5 μ l of the cDNA, 1 μ l of 10 mM deoxynucleotide triphosphohydroxylases, 0.3 μ l Platinum Taq DNA Polymerase High Fidelity, 5 μ l of 10X PCR buffer, 1.5 μ l of 50 mM MgSO₄, 36.7 μ l of H₂O, and 1 μ l each of 10 μ M forward and reverse primers (total volume of 50 μ l) were incubated at 94°C for 3 minutes followed by 35 cycles of the following: 94°C for 45 seconds, 54°C for 30 seconds, and 72°C for 1 minute. After the 35 cycles, the reaction was incubated at 72°C for 10 minutes for final extension. The primers amplify the region containing the deletion. For ENT1, the product size was 419 base pairs with a forward sequence of 5'-GAGGCTGGAGGG ACTGGGCTCC-3' and a reverse sequence of 5'-CAAGGGTGGCAG AGACAAGTGG-3'. Different reaction conditions and PCR buffer were necessary to amplify ENT2 because of high GC content. Briefly, 5 μ l of forward and reverse primers (10 μ M each), 1.5 μ l DMSO, 25 μ l 2 \times NEB Phusion High-Fidelity PCR Master Mix with GC Buffer, 3 μ l of cDNA, and 15.5 μ l of H₂O were incubated at 98°C for 30 seconds, and this was followed by 35 cycles of 98°C for 10 seconds, 68°C for 30 seconds, and 72°C for 30 seconds and a final extension of 10 minutes at 72°C. The product size was 794 base pairs with a forward sequence of 5'-GTGGGTTCCAGCTTTAGGGGTC-3' and a reverse sequence of 5'-GGGATCGGTGGGAAGGTCACCC-3'.

BlueJuice 10 \times gel loading buffer (Invitrogen, Carlsbad, CA) was added to the PCR product, and 45 μ l was loaded onto a 1% w/v agarose gel containing ethidium bromide and run for approximately 25 minutes at 130 V. PCR product was visualized using UV light, and bands corresponding to correct product sizes were excised and immediately extracted using Quantum Prep Freeze 'N Squeeze Gel Extraction Spin Columns (Biorad, Hercules, CA). Samples were submitted for Sanger sequencing at the University of Arizona Genetics Core.

Real-Time Quantitative PCR. cDNA was generated as described above and diluted 1:25 before real-time quantitative PCR. Each reaction contained 2 μ l of diluted cDNA, 5 μ l of PerfeCTa SYBR Green FastMix (Quantabio, Beverly, MA), 1 μ l each of 1 μ M forward and reverse primers, and 1 μ l of H₂O. Each reaction was performed in

duplicate per passage, with three passages for each cell line. The reaction conditions were 95°C for 5 minutes followed by 45 cycles of 95°C for 15 seconds and 60°C for 30 seconds using the Rotor-Gene RG-3000 (Corbett Research, San Francisco, CA). Specific primers for ENT1, ENT2, and GAPDH were designed using Primer3 software (Rozen and Skaletsky, 2000) to the 3' end of the genes, and primers were synthesized by Integrated DNA Technologies (Coralville, IA). The primers for ENT1 are located in exon 14 with a product size of 131 base pairs with a forward sequence of 5'-GCTGGGTCTGACCGTTGT AT-3' and a reverse sequence of 5'-CTGTACAGGGTGCATGATGG-3'. The primers for ENT2 are located in exon 12 with a product size of 164 base pairs, a forward sequence of 5'-AGCCTGCATGTGTGTA CTGC-3', and a reverse sequence of 5'-ACCACGGACCAGTCACTTTC-3'. The primers for GAPDH were a forward sequence of 5'-CGACCA CTTTGTCAAGCTCA-3' and a reverse sequence of 5'-CCCTGTTGC TGTAGCCAAAT-3'. Cycle threshold values (C_t) values relative to GAPDH expression levels in respective samples were used to determine expression levels of ENT1 and ENT2 using the $2^{-\Delta\Delta C_t}$ method (Livak and Schmittgen, 2001). Expression data are presented as mean fold change (\pm S.D.).

Cell Growth. Growth rate was assessed for wild-type HeLa S3 cells, ENT1 KO (ENT2) cells, and ENT2 KO (ENT1) cells. Cells were seeded at 30,000 cells/well in six-well plates, with duplicate wells per day of cell counting. Cells were counted daily using the Nexcelom Bioscience Cellometer Auto T4 cell counter for 5 days, and media were changed every other day. Doubling time was calculated from average cell count from two separate experiments.

Transport Experiments. Transport experiments were performed as previously described (Miller et al., 2020). All transport buffers were made with Waymouth's buffer (WB) (2.5 mM CaCl₂·2H₂O, 28 mM D-glucose, 13 mM HEPES, 135 mM NaCl, 1.2 mM MgCl₂, 0.8 mM MgSO₄·7H₂O, pH 7.4), 1 μ Ci/ml (approximately 20 nM) [³H]uridine, and selected test compounds. Test compound and transport buffer containing [³H]uridine were added to cells simultaneously with no preincubation of test compounds on cells. Inhibition of [³H]uridine uptake by NRTIs was tested at 100 μ M, 300 μ M, and 1 mM (Fig. 6; Supplemental Table 1). All compounds from Gilead Sciences Inc. arrived as 10 mM solutions in DMSO (Supplemental Table 2). Each compound (200 μ M each) was used for experiments to maximize the concentration of the compound used and to maintain below 2% final DMSO (v/v). All controls (100 nM and 100 μ M NBMPR; 200 μ M adenosine, guanosine, thymidine, inosine, and cytidine) contained 2% DMSO (v/v). Cells (200,000 cells/ml) were seeded into separate Nunc MicroWell 96-well optical bottom plates (Thermo-Fisher Scientific, Waltham, MA) for next-day experiments. Media were aspirated, and cells were washed once with 300 μ l of room temperature WB using a Biotek 405 LS Microplate Washer (BioTek, Winooski, VT) before initiating transport by adding 50 μ l of transport buffer containing compounds of interest and [³H]uridine using an Integra VIAFLO 96-well multichannel pipette (Integra Lifesciences, Plainsboro, NJ). Transport was terminated after 2 or 7 minutes as indicated in the figure legends by rinsing twice with WB. After washing, 200 μ l of MicroScint-20 scintillation cocktail (Perkin-Elmer, Waltham, MA) was added to each well before sealing with microplate film and incubated at room temperature in the dark for at least 2 hours. Total accumulated radioactivity was determined with a Wallac 1450 MicroBeta TriLux liquid scintillation counter (Perkin-Elmer, Waltham, MA).

Determination of Transport by Liquid Chromatography Tandem Mass Spectrometry. Transport experiments for liquid chromatography tandem mass spectrometry (LC-MS/MS) were completed as described above using 50 μ M of lexibulin, clofarabine, and cladribine for both cell lines; 50 μ M of nevirapine for ENT2 cells; and 100 μ M nevirapine for ENT1 cells. Uptake of compounds was measured in the presence or absence of 100 μ M NBMPR. Preliminary experiments determined that an incubation time of 5 minutes produced a detectable transport signal for these compounds; therefore, transport was terminated after 5 minutes. Samples were prepared as

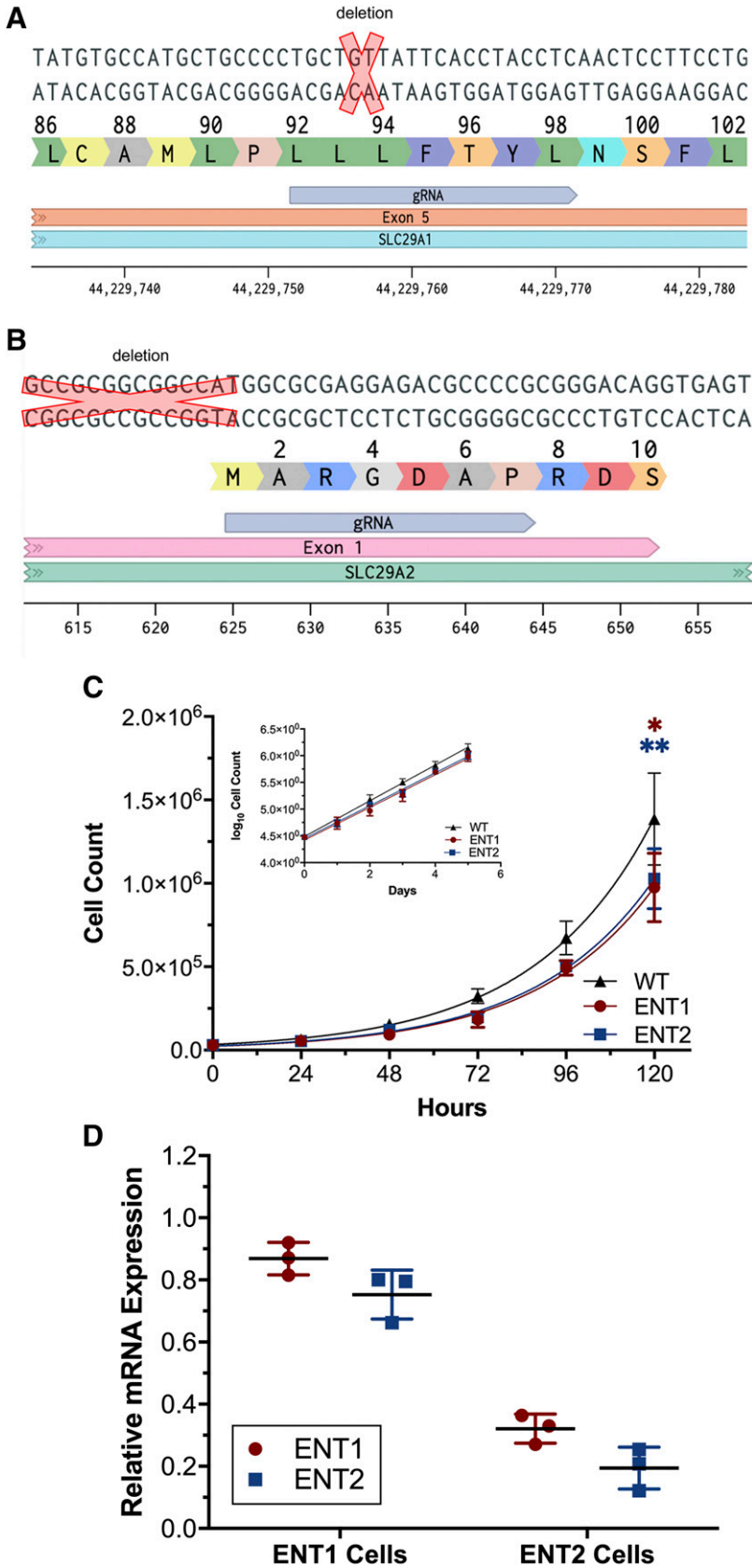


Fig. 1. Characterization of ENT1 and ENT2 KO cell lines. (A) Location of deletion in SLC29A1 exon 5 (red “x”) and gRNA used for generation of the ENT1 KO (ENT2) cells. (B) Location of deletion in SLC29A2 in exon 1 (red “X”) and gRNA used for generation of the ENT2 KO (ENT1) cells. DNA sequence 5’ to 3’ is shown for (A and B) as well as the amino acid sequence. (C) Growth curve of wild-type HeLa S3 cells and ENT1 and ENT2 cells. Log₁₀-transformed cell growth data are also plotted. Total cell count data were analyzed using two-way ANOVA with Sidak’s multiple comparisons test (**P* < 0.05; ***P* < 0.005, indicating difference from wild-type HeLa S3 cells). Data are presented as mean ± S.D. with *n* = 2 in duplicate. (D) Real-time PCR mRNA expression of ENT1 and ENT2 in ENT knockout cells relative to wild-type HeLa S3 cells. Relative ENT1 expression (red) and relative ENT2 expression (blue). Data are presented as mean ± S.D. with *n* = 3 in duplicate. WT, wild type.

described in (Miller et al., 2020). Briefly, after terminating transport, 50 μl of 1:1 methanol:ACN was added to cells containing 10 ng/ml of internal standard and incubated overnight at 4°C. The internal standard was abacavir for lexibulin and nevirapine. The internal standard for clofarabine was cladribine and vice versa. Calibration curves were also prepared in methanol:ACN and treated identically to samples. Samples were dried and resuspended in 50 μl of 90:10 H₂O:ACN + 0.1% formic acid for lexibulin and nevirapine and in 50 μl of H₂O + 0.1% formic acid for clofarabine and cladribine. Debris was removed by centrifuging at maximum speed for 10 minutes in a tabletop centrifuge, and the supernatant was collected for LC-MS/MS analysis.

A Shimadzu Prominence HPLC system (Shimadzu, Kyoto, Japan) coupled to a SCIEX QTRAP 4500 mass spectrometer (SCIEX, Framingham, MA) was used to detect intracellular accumulation of selected compounds. Clofarabine, cladribine, nevirapine, lexibulin, and abacavir were detected by positive electrospray ionization with the following source parameters: 5.5 kV ion spray voltage, 500°C source temperature, 20 psi nebulizer gas, 40 psi turbo gas, and 9 psi collision gas. Analyte intensity was determined by multiple reaction monitoring as noted in Supplemental Table 3. Ten microliters of each sample was injected onto a Luna Omega polar C18 column (50 \times 2.1 mm with 1.6 μm bead diameter; Phenomenex, Torrance, CA). For clofarabine and cladribine, analytes were separated over a binary gradient consisting of H₂O with 0.1% formic acid (A) and acetonitrile with 0.1% formic acid (B) at a flow rate of 0.3 ml/min as follows: 0% B (0 to 1 minute), 0%–80% B (1–5 minutes), held at 80% B for 1 minute, and this was followed by a decrease from 80% to 0% B (6–7.5 minutes). Lexibulin, nevirapine, and abacavir analytes were separated over a binary gradient consisting of water with 0.1% formic acid (A) and acetonitrile with 0.1% formic acid (B) at a flow rate of 0.3 ml/min as follows: 10% B (0–1 minute), 10%–90% B (1–3 minutes), 90% B (3–4 minutes), 90% to 10% B (4–4.5 minutes), and 10% B (4.5–6 minute).

Assay Central Bayesian Models. Assay Central software was used to build machine learning models and prediction generation methods and evaluate metrics of predictive performance and the interpretation of prediction and applicability scores as previously described (Clark et al., 2015; Clark and Ekins, 2015; Zorn et al., 2019). Initially, a series of scripts employing standardized rules was applied to detect problematic data (including abnormal valences and mixtures) and correct them by multiple methods (i.e., structures were desalted and neutralized, finite activities merged, potentially incorrect structures were flagged for review) to then output a high-quality structure-activity data set. A Bayesian algorithm was then applied to the structure-activity data sets generating extended-connectivity fingerprints 6 as molecular descriptors for structures, and the corresponding activity was either binary or set according to

a user-defined threshold for a Boolean classification (Clark et al., 2015; Clark and Ekins, 2015). The resulting machine learning model could be used to predict the probability of target activity from chemical structure alone. Prospective molecule applicability was evaluated by a score in which a higher value suggested higher fragment representation in the model to ensure a given prediction was within the scope of the training data. Prediction scores were evaluated according to the standard probability cutoff, wherein a value of ≥ 0.5 designates a chemical as active (Clark et al., 2015; Clark and Ekins, 2015).

Herein, we have applied Assay Central machine learning methods to ENT1 and ENT2 inhibition of [³H]uridine uptake into cells. Bayesian machine learning models were constructed from the percent uptake data generated from 44 unique compounds: 37 compounds provided in Supplemental Table 2 and five endogenous nucleosides as well as three tracers (two unique). Training data were binarized so that an active compound (i.e., an inhibitor of ENT1 or ENT2) was considered one that inhibited >50% average [³H]uridine uptake. No structural corrections were necessary.

Additionally, we externally validated a machine learning model built from ChEMBL IC₅₀ data to evaluate whether machine learning could correctly predict the ENT1 results generated in this study. Specifically, training data were pulled from Target identification 1997 (https://www.ebi.ac.uk/chembl/target_report_card/CHEMBL1997/) for human ENT1, and the activity threshold was set so that a compound was considered active if the reported IC₅₀ was <100 μM . The two test sets were comprised of all compounds (Supplemental Table 2), five endogenous nucleosides, and three additional compounds; all compounds had percent uptake, and 27 had estimated-IC₅₀ data against ENT1. Estimated-IC₅₀ values were calculated using eq. 4, and uptakes were determined in the absence of inhibitor and in the presence of each inhibitor at 200 μM . Five compounds were in the training model ([³H]uridine + 5 mM uridine, [³H]uridine + 100 nM NBMPR, [³H]uridine + 100 μM NBMPR adenosine, and tecadenoson), and they were removed from this test set. Testing compounds were binarized so that an active compound was considered one that produced <50% of control uptake or an estimated IC₅₀ < 100 μM . External validation, which we term a “subvalidation,” was applied within Assay Central so that the binarized ChEMBL training set was applied to predict each individual test set and output performance metrics. Individual predictions that culminate in these metrics are provided in Supplemental File 1 with the five removed compounds noted as “In model” for the applicability score. Only minimal structural corrections were necessary (i.e., removing salt components, omitting 49 compounds that did not provide an IC₅₀ value). Additional information on the generation of Assay Central Bayesian Models is included in the Supplemental Files under “Assay Central® User Manual” of Sandoval et al. (2018).

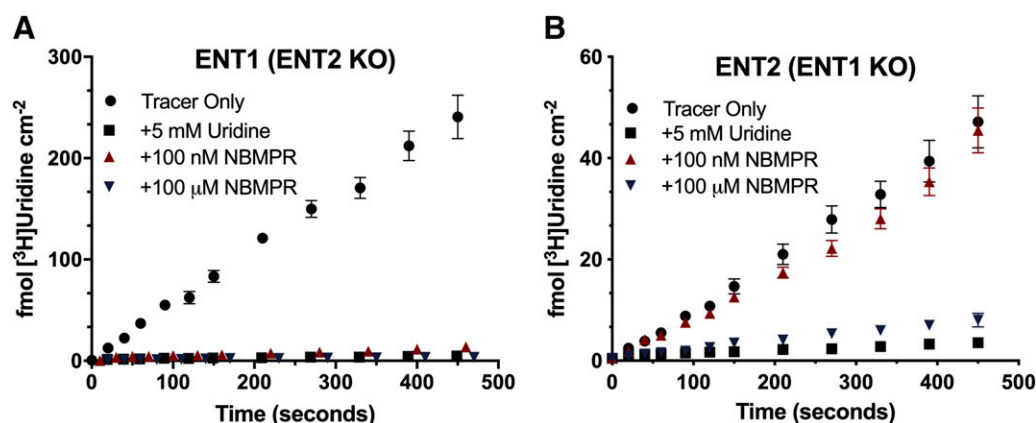


Fig. 2. Inhibition of [³H]uridine uptake in ENT2 and ENT1 knockout cell lines. Approximately 20 nM [³H]uridine was incubated with 5 mM uridine (black square), 100 nM NBMPR (red triangle), or 100 μM NBMPR (blue triangle) in the ENT1 cell line [ENT2 KO, (A)] and the ENT2 [ENT1 KO, (B)] up to 7 minutes. Total accumulated [³H]uridine was measured. Data are represented as mean \pm S.D. with $n = 3$ in triplicate.

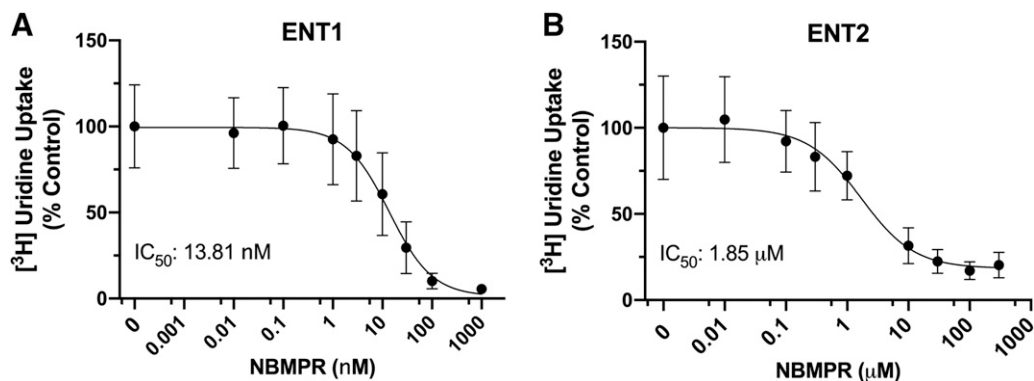


Fig. 3. NBMPR IC_{50} curves in ENT1 (A) and ENT2 (B) cell lines. Approximately 20 nM [3H]uridine was incubated with increasing concentrations of NBMPR. Total accumulated [3H]uridine was measured after 2 minutes. Results were normalized to total accumulated [3H]uridine in the absence of NBMPR. Equation 2 was used to generate IC_{50} values for each experiment. Data are represented as mean \pm S.D. with $n = 3$ in triplicate.

Data Analysis. Each experiment was completed with cells cultured from multiple passages and multiple replicates per passage as indicated in the figure legends and predetermined before conducting the experiment. Data are presented as mean \pm S.D. unless otherwise noted and completed using GraphPad Prism 8 (San Diego, CA). For analysis of cell growth data, two-way ANOVA with Sidak's correction for multiple comparisons (12 comparisons per family) was used to compare the mean cell count of knockout cells to wild-type cells ($P < 0.05$). Doubling time was calculated by fitting the exponential growth equation to cell growth data:

$$\text{Doubling time} = Y_0 e^{k \cdot X} \quad (1)$$

in which Y_0 is the initial amount of cells seeded (30,000), X is hours, and k is the rate constant.

The IC_{50} value of NBMPR, abacavir, nevirapine, lexibulin, clofarabine, and cladribine on ENT1- and ENT2-mediated [3H]uridine uptake was determined using the following equation:

$$J = \frac{J_{app} \cdot [T]}{IC_{50} + [S]} + K_d \cdot [T] \quad (2)$$

in which J is total uridine transport, J_{app} is a constant (J_{max} for uridine times the ratio of the IC_{50} for the inhibitor and the K_t for uridine), T is [3H]uridine concentration, and S is NBMPR concentration. We estimated the initial rate of uridine uptake at 2 minutes. The nonsaturable/mediated component of total net accumulation, K_d , was determined using eq. 3a and has units of $\mu\text{l} \cdot \text{cm}^{-2} \cdot \text{min}^{-1}$. This value was subtracted from total uridine uptake at each substrate

concentration to generate values for J_{max} and K_t (eq. 3b), as previously described for wild-type HeLa cells (Miller et al., 2020):

$$J = \frac{J_{max} \cdot [S]}{K_t + [S]} + K_d \cdot [S] \quad (3a)$$

$$J = \frac{J_{max} \cdot [S]}{K_t + [S]} \quad (3b)$$

An unpaired two-tailed t test was used to calculate the statistical difference between each kinetic parameter, NBMPR IC_{50} values, and transport determination studies ($P < 0.05$ indicating a difference in kinetic parameters or NBMPR IC_{50} values, $P > 0.05$ indicating no difference). An extra sum-of-squares F-test and comparison of fits were used to calculate the statistical difference between IC_{50} values generated from best-fit lines for endogenous nucleosides and estimated- IC_{50} values for nucleoside analog/heterocycle analog interaction studies ($P < 0.05$ indicating an difference in IC_{50} values between ENT1 and ENT2, $P > 0.05$ indicating no difference). Data in Tables 2–4 are presented as mean and 95% confidence intervals. Ordinary one-way ANOVA with Dunnett's correction for multiple comparisons comparing the mean of a column to the control column (i.e., [3H]uridine uptake only) was used for experiments with NRTIs (Fig. 6) and nucleoside/heterocycle analogs (Fig. 7). For nucleoside/heterocycle analogs that inhibited [3H]uridine uptake, a comparison of fits of eq. 4 and extra sum-of-squares F-test were done to compare the values for each cell line. IC_{50} values for these compounds were estimated from inhibition experiments using eq. 4 as previously described (Kido et al., 2011; Sandoval et al., 2018):

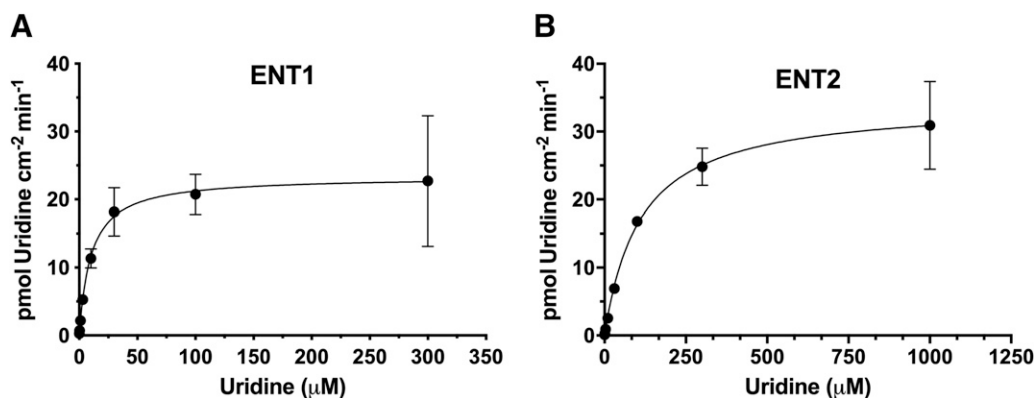


Fig. 4. Uridine kinetics in ENT1 (A) and ENT2 (B) cell lines. Twenty nanomolars [3H]uridine uptake in the presence of increasing amounts of unlabeled uridine was measured after 2 minutes. Michaelis-Menten kinetics (eq. 3) were used to generate kinetic parameters in Table 2. The nonsaturable component was subtracted from total accumulated [3H]uridine. Data are represented as mean \pm S.D. with $n = 3$ in triplicate.

TABLE 1

Kinetic parameters of ENT2 and ENT1 knockout cell lines

An unpaired *t* test was used to determine significance ($P < 0.05$). All data are represented as mean \pm S.D. with $n = 3$.

	ENT1 Uridine Uptake	ENT2 Uridine Uptake	<i>P</i> Value	Ratio ENT2:ENT1
J_{\max} (pmol cm ⁻² min ⁻¹)	23.75 \pm 0.88	44.88 \pm 16.34	0.089	1.89
K_t (μ M)	11.36 \pm 3.87	156.90 \pm 55.60	0.016	13.81

$$J = \frac{J_0}{1 + \frac{I}{\text{Estimated } IC_{50}}} \quad (4)$$

in which J_0 represents ENT-mediated transport rate in the absence of the inhibitor, and J represents ENT-mediated transport rate in the presence of the inhibitor. I is the inhibitor concentration (200 μ M).

Results

Generation and Characterization of ENT1 and ENT2

Knockout Cell Lines. Successful deletion of ENT1 and ENT2 was confirmed in HeLa S3 cells using PCR and Sanger sequencing. Figure 1, A and B show the location of the deletions in each cell line. For the ENT1 KO cells, there is a two-nucleotide deletion in exon 5. For the ENT2 KO cells, there is a 14 nucleotide deletion in exon 1. Hereafter, these cell lines are referred to as ENT1 or ENT2 cells, named after the transporter that remains functional. Cell growth of the newly generated cell lines was also assessed. After 5 days in culture, both cell lines had a lower total cell count than wild-type HeLa S3 cells (Fig. 1C) ($P < 0.001$ for ENT1 cells, $P < 0.05$ for ENT2 cells). The doubling time was calculated using eq. 1. For wild-type HeLa cells, the doubling time was 22.78 hours (95% CI: 18.47–27.95). For ENT1 cells, the doubling time was 22.0 hours (95% CI: 17.55–27.41). For ENT2 cells, the doubling time was 22.14 hours (95% CI: 18.43–26.48). The mRNA expression levels were measured in both knockout cell lines

relative to wild-type HeLa cells (Fig. 1D). The mRNA expression of ENT1 and ENT2 modestly decreased relative to wild-type cells in the ENT1 cells. However, in ENT2 cells, mRNA expression of both ENT1 and ENT2 decreased relative to wild-type cells.

Functional Assessment of ENT1 and ENT2 Cell Lines.

We measured the accumulation of [³H]uridine over the course of 7 minutes in both cell lines to evaluate the functional loss of ENT1 or ENT2. A saturating concentration of unlabeled uridine (5 mM) was used to establish the fraction of total uridine accumulation that was carrier-mediated. Although there was only a modest decrease in mRNA expression of ENT2, >96% of [³H]uridine uptake was mediated by ENT1 in ENT1 cells (Fig. 2A). In ENT2 cells, >90% of [³H]uridine uptake was mediated by ENT2 (Fig. 2B). The IC_{50} of NBMPR for each transporter was determined using eq. 2. For ENT1, the IC_{50} was 13.81 (95% CI: -0.104 to 28.66) nM, and for ENT2, the IC_{50} was 1.85 (95% CI: 0.245–3.44) μ M (Fig. 3, $P = 0.0078$).

Kinetics of Uridine Transport. [³H]uridine uptake was effectively linear for 7 minutes in wild-type HeLa cells and in the ENT1 and ENT2 cells (Miller et al., 2020). To determine uridine transport kinetics in each cell line, we evaluated [³H]uridine uptake after 2 minutes to estimate the initial rate of uptake. The J_{\max} for ENT1 was 23.8 \pm 0.9 pmol·cm⁻²·min⁻¹, and for ENT2 it was 44.9 \pm 16.3 pmol·cm⁻²·min⁻¹ ($P = 0.089$). The K_t for ENT1 was 13.8-fold lower than that for ENT2

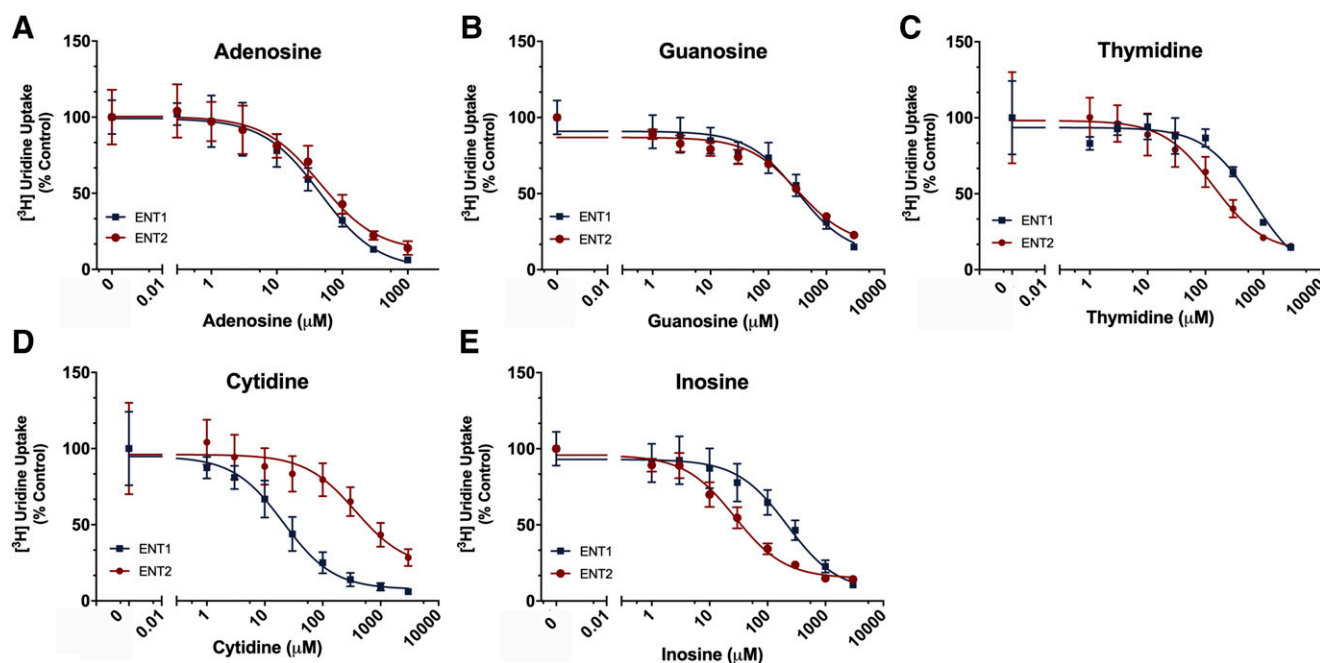


Fig. 5. Endogenous nucleoside [³H]uridine uptake in ENT1 and ENT2 cell lines. Inhibition of [³H]uridine uptake in the presence of endogenous nucleosides in ENT1 (blue squares) and ENT2 (red circles) cell lines by Adenosine (A), Guanosine (B), Thymidine (C), Cytidine (D) and Inosine (E). Equation 2 was used to generate best-fit lines, and IC_{50} values are reported in Table 3. All data are represented as mean \pm S.D. with $n = 3$ in triplicate.

TABLE 2

IC₅₀ values of endogenous nucleosides in ENT1 and ENT2 cell linesBest-fit values from eq. 2 were compared using the extra sum-of-squares *F*-test to determine significance. IC₅₀ values are represented as mean and 95% C.I. with *n* = 3. Significance is indicated next to the compound name on the table (***P* < 0.001; ****P* < 0.0001).

Nucleoside	ENT1 IC ₅₀ (μM)	ENT2 IC ₅₀ (μM)	<i>P</i> Value	Ratio ENT2:ENT1
Adenosine	39.92 (95% CI: 24.5–65.1)	56.55 (95% CI: 29.3–108.5)	0.377	1.42
Guanosine	385.90 (95% CI: 194.4–780.5)	254.90 (95% CI: 140.5–458.6)	0.358	0.66
Thymidine**	708.90 (95% CI: 368.6–1468)	138.10 (95% CI: 64.7–290.4)	0.0014	0.19
Inosine***	219.50 (95% CI: 113.1–426.4)	27.02 (95% CI: 19.5–37.49)	<0.0001	0.12
Cytidine***	21.08 (95% CI: 12.2–36.7)	368.20 (95% CI: 105.3–1338)	<0.0001	17.47

(11.4 ± 3.9 and 156.9 ± 55.6 μM, *P* = 0.016) (Fig. 4; Table 1). The ratios of the kinetic parameters are also presented in Table 1.

Endogenous Nucleoside Interactions. We examined the differences in inhibition of [³H]uridine uptake in the ENT1 and ENT2 cell lines determined in the presence of the endogenous nucleosides: adenosine, guanosine, thymidine, inosine, and cytidine (Fig. 5; Table 2). A best-fit line was generated from eq. 2 to generate IC₅₀ values, and an extra sum-of-squares *F*-test (*P* < 0.05 indicating a statistical difference in IC₅₀ values, *P* > 0.05 indicating no statistical difference in IC₅₀ values) was used for comparison. For adenosine, the IC₅₀ was 39.9 (95% CI: 24.5–65.14) μM for ENT1 and 56.5 (95% CI: 29.3–108.5) μM for ENT2 (*P* = 0.3767). For guanosine, the IC₅₀ for ENT1 was 385.9 (95% CI: 194.4–780.5) μM and 254.9 (95% CI: 140.5–458.6) μM for ENT2 (*P* = 0.3582). The IC₅₀ value for thymidine was 5.1-fold lower for ENT2 than ENT1: 138.1 (95% CI: 64.7–290.4) μM and 708.9 (95% CI: 368.6–1468.0) μM, respectively (*P* = 0.0014). The IC₅₀ for inosine was 8.1-fold lower for ENT2 than ENT1 [27.0 (95% CI: 19.5–37.5) μM and 219.5 (95% CI: 113.1–426.4) μM, *P* < 0.0001]. The IC₅₀ for cytidine was 17.5-fold lower for ENT1 than ENT2 [21.1 (95% CI: 12.2–36.7)

μM and 368.2 (95% CI: 105.3–1338.0) μM, *P* < 0.0001]. The ratios of the IC₅₀ values for ENT2 and ENT1 are shown in Table 2.

NRTI Interactions. Nine NRTIs (abacavir, zidovudine, entecavir, zalcitabine, lamivudine, emtricitabine, didanosine, stavudine, and tenofovir disoproxil) (Fig. 6; Supplemental Table 1) were evaluated for their impact on [³H]uridine uptake. The selected NRTIs have molecular weights below 300 g/mol except tenofovir disoproxil. These NRTIs were tested at 100 μM, 300 μM, and 1 mM in Fig. 6 as previously described (Miller et al., 2020). Only abacavir inhibited [³H]uridine uptake at all three concentrations for both cell lines. Zidovudine inhibited uptake at 300 μM and 1 mM in both cell lines. Entecavir inhibited [³H]uridine uptake at 1 mM in ENT2 cells. Emtricitabine modestly inhibited uptake at all concentrations in ENT2 cells. Since abacavir was the most potent inhibitor of the nine NRTIs tested, we determined its IC₅₀ for ENT1 and ENT2 (Fig. 8A). IC₅₀ values of abacavir were 85.7 (95% CI: 34.2, 137.3) μM for ENT1 and 316.8 (95% CI: 113.3, 520.2) μM for ENT2 (*P* = 0.0056).

Nucleoside/Heterocycle Analog Interactions. Thirty-seven nucleoside/heterocycle analogs (Supplemental Table 2)

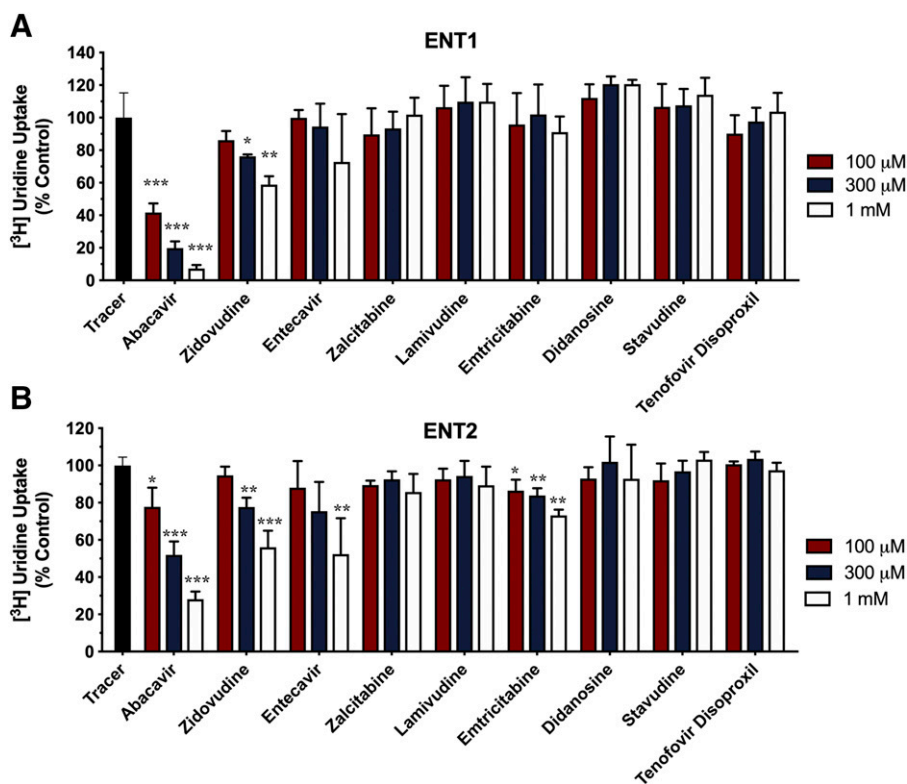


Fig. 6. NRTI inhibition of [³H]uridine uptake in ENT1 and ENT2 cell lines. Approximately 20 nM of [³H]uridine uptake was incubated with 100 μM (red bars), 300 μM (blue bars), or 1 mM (white bars) of nine different NRTIs for 2 minutes with ENT1 (A) or ENT2 (B) cell lines. The black bar represents tracer 20 nM [³H]uridine only. Amount of [³H]uridine uptake was normalized to percentage of uptake in tracer-only condition. Ordinary one-way ANOVA with Bonferroni's correction for multiple comparisons to a control column (i.e., [³H]uridine only) with three comparisons per family and **P* < 0.05; ***P* < 0.01; ****P* < 0.0001 was used.

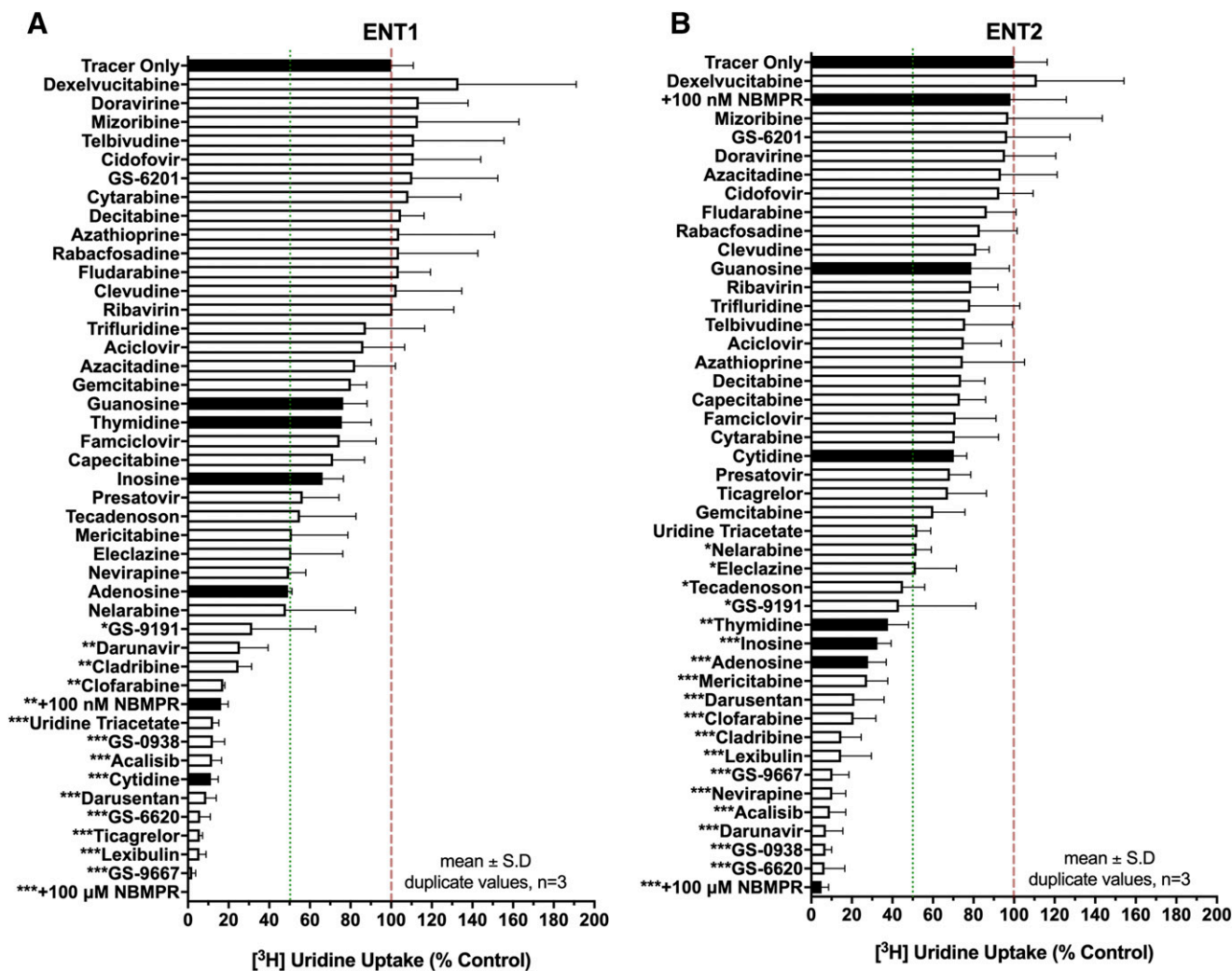


Fig. 7. Nucleoside/heterocycle analog inhibition of ENT-mediated [^3H]uridine uptake in ENT1 (A) and ENT2 (B) cell lines. Structures are provided in Supplemental Fig. 1. Approximately 20 nM of [^3H]uridine was incubated with 200 μM of 37 different nucleoside/heterocycle analogs (white bars) for 2 minutes in each cell line. The black bars represent 200 μM endogenous nucleosides, 100 nM NBMPR, and 100 μM NBMPR. Ordinary one-way ANOVA with Dunnett's correction for multiple comparisons ($P < 0.05$ indicating a difference from control) was used for statistical analyses of these experiments. Significance is indicated by the compound name on the y-axis (* $P < 0.05$; ** $P < 0.01$; *** $P < 0.001$). Data are represented as mean \pm S.D from duplicate values with $n = 3$.

were tested at 200 μM to evaluate their impact on [^3H]uridine uptake (Fig. 7). This concentration was used to maximize the concentration of the compound used while still remaining below 2% DMSO (v/v) to prevent interference with transport. Seventeen compounds inhibited uptake in at least one cell line. For ENT1, estimated- IC_{50} values ranged from 4 to 209 μM , and for ENT2, estimated- IC_{50} values ranged from 23 to 441 μM . Nevirapine, ticagrelor, and uridine triacetate had different estimated- IC_{50} values for ENT1 and ENT2 ($P = 0.0026$, $P = 0.0007$, and $P = 0.0013$, respectively, Table 3). The ratios of the estimated- IC_{50} values for ENT2 and ENT1 are shown in Table 3. Using this method to estimate IC_{50} values, thymidine, inosine, and cytidine had differing values for ENT1 and ENT2 ($P = 0.0152$, $P = 0.014$, $P = 0.0001$, respectively) that reflected the results from full IC_{50} curves in Fig. 5. Full IC_{50} values were determined for nevirapine, lexibulin, clofarabine, and cladribine using eq. 2 (Fig. 8, B–E). Nevirapine inhibited 50% of [^3H]uridine uptake for ENT1 at 166.8 μM (95% CI: -32.88 to 366.6) and 17.78 μM (95% CI: 2.83–32.73) for ENT2

($P = 0.011$). Lexibulin inhibited 50% of [^3H]uridine uptake for ENT1 at 16.49 μM (95% CI: 0.776–32.20) and 21.32 μM (95% CI: -2.24 to 44.89) for ENT2 ($P = 0.722$). Clofarabine inhibited 50% of [^3H]uridine uptake for ENT1 at 31.48 μM (95% CI: 11.83–51.13) and 12.22 μM (95% CI: 2.53–21.91) for ENT2 ($P = 0.051$). Cladribine inhibited 50% of [^3H]uridine uptake for ENT1 at 67.26 μM (95% CI: 28.10–106.40) and 40.15 μM (95% CI: 15.06–65.24) for ENT2 ($P = 0.170$).

Transport Determination for Nevirapine, Lexibulin, Clofarabine, and Cladribine. Accumulation of clofarabine, cladribine, nevirapine, and lexibulin was measured in the absence and presence of NBMPR and detected by LC-MS/MS (Fig. 9). A decrease in clofarabine uptake was detected in the presence of NBMPR in ENT1 and ENT2 cells ($P = 0.026$, $P = 0.0482$). Similarly, a decrease in cladribine uptake was detected in the presence of NBMPR in ENT1 and ENT2 cells ($P = 0.0031$, $P = 0.0096$). No change in nevirapine uptake in the presence of NBMPR was detected in ENT1 or ENT2 cells ($P = 0.1502$, $P = 0.9691$). No change in lexibulin uptake was

TABLE 3

Estimated-IC₅₀ values of nucleoside/heterocycle analogs that inhibited [³H]uridine uptake in ENT1 and ENT2 cell lines

Endogenous nucleoside estimated-IC₅₀ values are also included. Values are ranked from lowest to highest in the ENT1 cells. IC₅₀ values were generated from two data points: tracer only (0 μM) and 200 μM using eq. 4. A comparison of fits for the IC₅₀ equation extra sum-of-squares *F*-test was done to compare the estimated-IC₅₀ values for each cell line (**P* < 0.05). Estimated-IC₅₀ values are presented as mean and 95% C.I. with *n* = 3.

Analog	ENT1 Estimated IC ₅₀ (μM)	ENT2 Estimated IC ₅₀ (μM)	Ratio ENT2:ENT1
GS-9667	4.3 (95% CI: -18.87 to 34.45)	24.0 (95% CI: -15.9 to 89.22)	5.58
Lexibulin	12.0 (95% CI: -13.4 to 46.1)	35.3 (95% CI: -16.8 to 139.2)	2.94
Ticagrelor*	12.4 (95% CI: -12.4 to 45.2)	441.1 (95% CI: 128.1 to infinity)	35.57
GS-6620	12.7 (95% CI: -14.2 to 49.4)	14.2 (95% CI: -24.5 to 77.2)	1.12
Darusentan	19.9 (95% CI: -8.6 to 59.3)	55.5 (95% CI: -4.2 to 185.9)	2.79
Acalisib	27.1 (95% CI: -2.8 to 69.3)	20.6 (95% CI: -17.9 to 82.6)	0.76
GS-0938	28.0 (95% CI: -3.3 to 72.8)	15.4 (95% CI: -18.4 to 66.1)	0.55
Uridine triacetate*	28.4 (95% CI: -0.5 to 68.5)	228.7 (95% CI: 102.3 to 656.0)	8.05
Clofarabine	42.2 (95% CI: 10.7 to 87.0)	54 (95% CI: 0.44 to 159.2)	1.28
Cladribine	66.1 (95% CI: 23.3 to 135.1)	35.7 (95% CI: -9.8 to 116.2)	0.54
Darunavir	68.8 (95% CI: 11.9 to 182.2)	15.8 (95% CI: -21.8 to 75.69)	0.23
GS-9191	180.4 (95% CI: 30.39 to 1723)	391.1 (95% CI: 108.8 to infinity)	2.17
Nelarabine	186.3 (95% CI: 15.9 to 3480)	225.2 (95% CI: 99.0 to 659.3)	1.21
Nevirapine*	198.3 (95% CI: 100.8 to 434.4)	23.7 (95% CI: -14.7 to 85.3)	0.12
Eleclazine	207.6 (95% CI: 47.5 to 2934)	222.6 (95% CI: 60.96 to 2107)	1.07
Mericitabine	209.8 (95% CI: 41.31 to 11447)	78.1 (95% CI: 16.2 to 209.4)	0.37
Tecadenoson	245.9 (95% CI: 52.7 to infinity)	171.8 (95% CI: 65.7 to 510.7)	0.70
Adenosine	194.1 (95% CI: 112.3 to 357.0)	80.2 (95% CI: 19.4 to 205.9)	0.41
Guanosine	646.9 (95% CI: 250.2 to infinity)	830.2 (95% CI: -infinity to infinity)	1.28
Thymidine*	624.4 (95% CI: 221.6 to infinity)	126.0 (95% CI: 43.4 to 338.0)	0.20
Inosine*	394.0 (95% CI: 182.0 to 1601.0)	100.0 (95% CI: 34.3 to 238.5)	0.25
Cytidine*	25.6 (95% CI: -3.2 to 65.5)	507.9 (95% CI: 209.2 to 7457)	19.84

observed in the presence of NBMPR in ENT1 cells (*P* = 0.1589), but an increase in uptake was detected in the presence of NBMPR in ENT2 cells (*P* = 0.0340).

Assay Central Bayesian Models. Bayesian models were generated for ENT1 and ENT2 using percent uptake of control (i.e., [³H]uridine uptake only) in the presence of 37 nucleoside analogs (200 μM), 5 mM uridine, 100 μM NBMPR, and five endogenous nucleosides (200 μM) for a total of 44 compounds in each model. Inhibitors were classified as “active” if uptake was reduced by at least 50%; there were 18 active compounds for ENT1 and 17 active compounds for ENT2. Both the ENT1 and ENT2 models (Fig. 10) performed similarly and produced high performance metrics. Receiver operator characteristic (ROC) scores exceeded 0.71, with recall and specificity metrics ranging from 0.69 to 0.77. For small data sets, these scores are acceptable. The truth tables below the ROC curves indicate the number compounds that were of true positive (predicted and are inhibitors), false positive (type 1 error; predicted to be inhibitors and were not), true negative (were not predicted and are not inhibitors), and false negative (type 2 error; were not predicted and were inhibitors). Additional statistics presented in Figs. 10 and 11 include 1) precision, 2) recall (sensitivity; i.e., true positive rate), 3) specificity (i.e., true negative rate), 4) F1 score, 5) κ , and 6) Matthews correlation coefficient (MCC) (i.e., overall model classification performance). Equations and descriptions for these parameters for

model statistics are previously described (Cohen, 1960; Matthews, 1975; Carletta, 1996; Zorn et al., 2019). These common metrics for evaluating machine learning model performance indicate that future prospective predictions can be reasonably considered, as the internal predictive performance is better than random chance.

External validation or Assay Central subvalidations were also performed for ENT1, in which test set compounds were classified as inhibitors if the prediction thresholds were above 0.5. The ENT1 training model was built from all IC₅₀ data available from ChEMBL Target ID 1997, and the threshold was set at 100 μM (Fig. 11A). The estimated-IC₅₀ values were calculated from the rates of transport measured in the absence of inhibitor and in the presence of 200 μM concentrations of a battery of test inhibitor compounds (II), i.e., J₀ and J_i, respectively, using the eq. 4 (Kido et al., 2011; Sandoval et al., 2018). These calculated values are referred to as “estimated” IC₅₀ values. The test set was composed of the 37 nucleoside/heterocycle analogs, endogenous nucleosides, and NBMPR and uridine, with percent uptake and estimated-IC₅₀ data generated using eq. 4 using two points: [³H]uridine and 200 M of compound. Five compounds were in the training model (adenosine, [³H]uridine + 5 mM uridine, [³H]uridine + 100 nM NBMPR, [³H]uridine + 100 μM NBMPR, and tecadenoson), so they were removed from the test set. The individual predictions summarized in the truth table for each transporter test

TABLE 4

IC₅₀ values of abacavir, nevirapine, lexibulin, clofarabine, and cladribine in ENT1 and ENT2 cell lines

Best-fit values from eq. 2 were compared using the extra sum-of-squares *F*-test. IC₅₀ values presented as mean and 95% C.I. with *n* = 3 and significance denoted by **P* < 0.05 and ** *P* < 0.01.

Nucleoside	ENT1 IC ₅₀ (μM)	ENT2 IC ₅₀ (μM)	<i>P</i> Value	Ratio ENT2:ENT1
Abacavir**	85.74 (95% CI: 34.22 to 137.3)	316.8 (95% CI: 113.3 to 520.2)	0.0056	3.69
Nevirapine*	166.8 (95% CI: -32.88 to 366.6)	17.78 (95% CI: 2.83 to 32.73)	0.0113	0.11
Lexibulin	16.49 (95% CI: 0.776 to 32.20)	21.32 (95% CI: -2.24 to 44.89)	0.722	1.29
Clofarabine	31.48 (95% CI: 11.83 to 51.13)	12.22 (95% CI: 2.53 to 21.91)	0.0509	0.39
Cladribine	67.26 (95% CI: 28.1 to 106.4)	40.15 (95% CI: 15.06 to 65.24)	0.1703	0.60

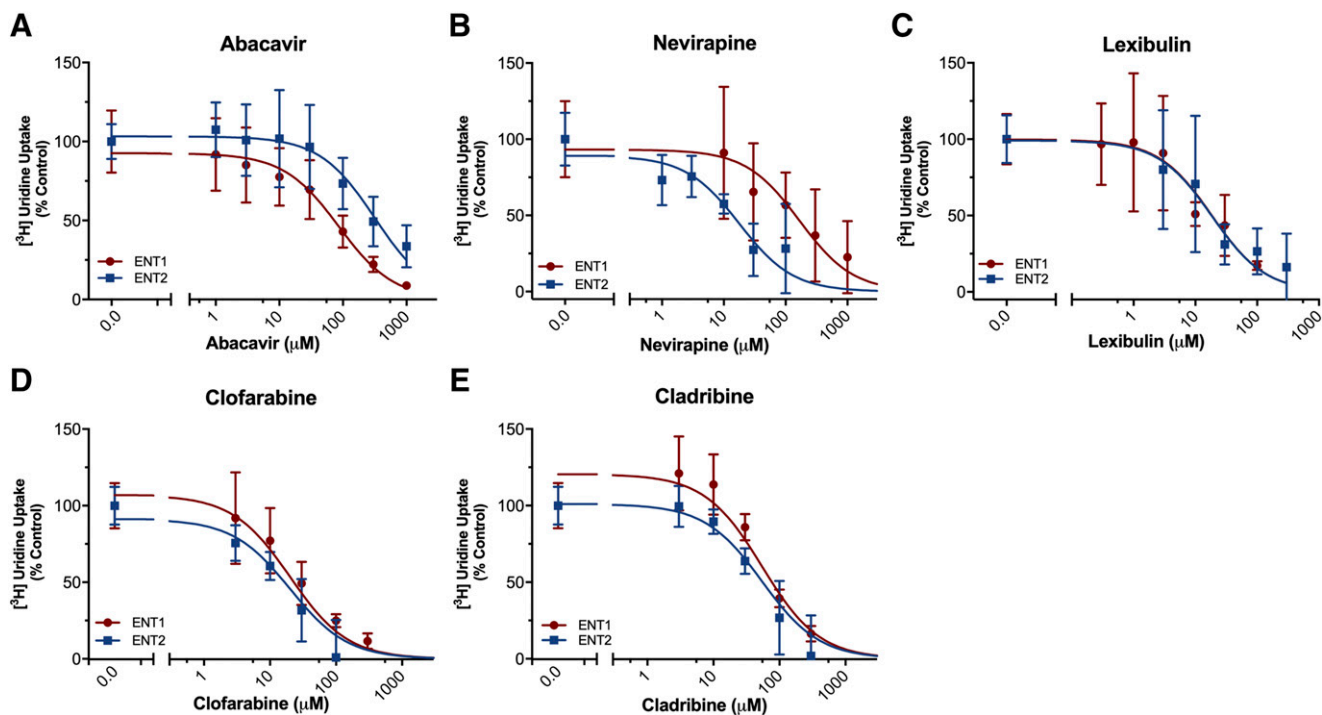


Fig. 8. Inhibition of [^3H]uridine uptake in the presence of abacavir (A), nevirapine (B), lexibulin (C), clofarabine (D), and cladribine (E) in ENT1 (red circles) and ENT2 (blue squares) cell lines. IC_{50} values are reported in Table 4. Data are reported as mean [^3H]uridine uptake as a percentage of control (i.e., in absence of compound) \pm S.D. with $n = 3$ in duplicate.

set have also been made available (Supplemental File 1). The first test set for ENT1 subvalidation (Fig. 11B) was defined by binary classification of percentage uptake less than 50%, totaling 40 compounds. The public training data set correctly predicted 58% of inhibitors. The second test set for ENT1 subvalidation (Fig. 11C) was defined by binary classification of estimated- IC_{50} values of less than 100 μM with 27 compounds total. In this case, the public training data set correctly predicted 63% of test set inhibitors.

Discussion

This study generated CRISPR/Cas9 functional knockouts of ENT1 and ENT2 in HeLa S3 cells with deletions in exon 5 and exon 1, respectively (Fig. 1A). In ENT1 cells, >96% of [^3H]uridine uptake was mediated by ENT1 (Fig. 2A). In ENT2 cells, 90% of [^3H]uridine uptake was mediated by ENT2 (Fig. 2B). The ENT1 cells showed approximately 2.4 times the ENT1-mediated [^3H]uridine uptake observed in wild-type HeLa S3 cells when ENT activity was pharmacologically separated using NBMPR and 1.8 times the amount of total combined ENT1- and ENT2-mediated [^3H]uridine uptake (Miller et al., 2020). The ENT2 cells showed approximately 1.4 times the observed ENT2-mediated [^3H]uridine uptake in wild-type HeLa S3 cells (Miller et al., 2020). There were no differences in the growth rate of wild-type and ENT cells (Fig. 1C). We saw decreases in ENT1 and ENT2 mRNA expression for ENT2 cells and modest decreases in mRNA expression of ENT1 and ENT2 in ENT1 cells (Fig. 1D). Increase in [^3H]uridine uptake may be attributed to increased protein expression or function of the remaining functional transporter. However, we have

not been able to find reliable antibodies for ENT1 and ENT2 to assess this.

There was a 13.8-fold difference in the K_t for ENT1 and ENT2 that aligns with observations in wild-type HeLa S3 cells (reported K_t of 13.6 and 108.9 μM , respectively) (Miller et al., 1978; Plagemann and Wohlhueter, 1984; Boleti et al., 1997; Ward et al., 2000; Miller et al., 2020). The data confirm that CRISPR/Cas9 functional knockout of natively expressed ENTs in HeLa cells results in transport activity of the remaining homology that retains quantitatively similar characteristics as those expressed in other natively expressing model systems.

In studies with endogenous nucleosides, cytidine had the highest affinity for ENT1, and inosine had the highest affinity for ENT2. Thymidine had a higher affinity for ENT1 than ENT2, whereas guanosine and adenosine did not have differences in affinity for each transporter, similar to previously reported values using wild-type HeLa cells and NBMPR (Miller et al., 2020). However, the authors did not observe a difference between the IC_{50} values of thymidine for ENT1- and ENT2-mediated [^3H]uridine uptake (Miller et al., 2020). These knockout cell lines assisted with the differentiation of this parameter for thymidine and could assist in delineating ENT1 or ENT2 affinity for other compounds.

In our studies with nucleoside reverse-transcriptase inhibitors, abacavir inhibited both ENT1- and ENT2-mediated [^3H]uridine uptake, whereas zidovudine, entecavir, and emtricitabine inhibited ENT2 at a lower concentration than ENT1.

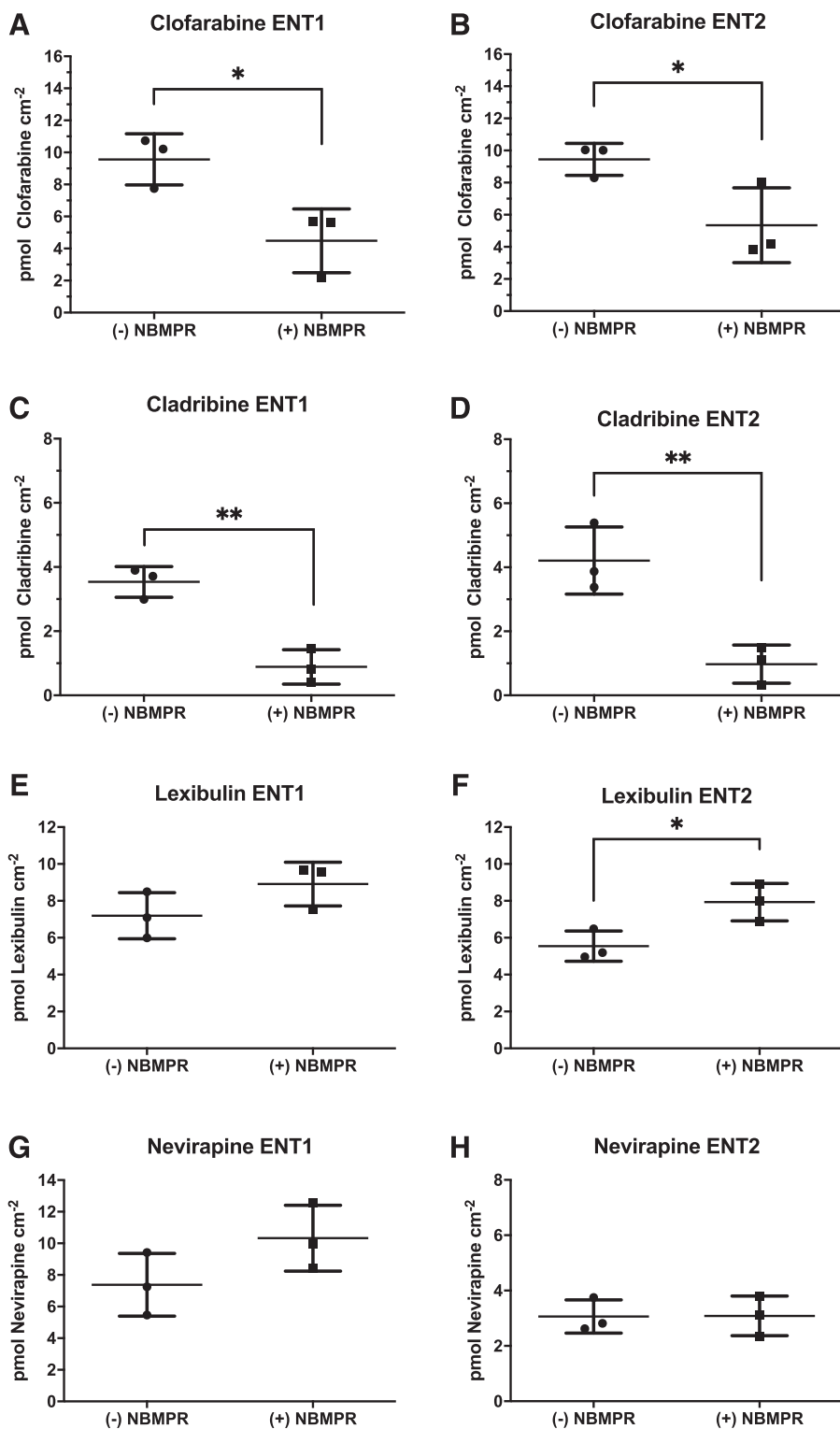


Fig. 9. Determination of transport for identified inhibitors of [³H]uridine uptake in ENT1 and ENT2 cell lines. Total accumulation of clofarabine (A and B), cladribine (C and D), lexibulin (E and F), and nevirapine (G and H) over 5 minutes measured in the absence and presence of 100 μM NBMPR in ENT cells detected by LC-MS/MS. Fifty micromolars lexibulin, clofarabine, and cladribine were used for both cell lines, and nevirapine was used for ENT2 cells. One-hundred micromolars nevirapine was used for ENT1 cells. Data are reported as mean ± S.D. with *n* = 3 in duplicate (**P* < 0.05; ***P* < 0.01)

Abacavir and entecavir are both guanosine analogs; however, guanosine appears to be a relatively low-affinity substrate for both ENT1 and ENT2 (Miller et al., 2020). We previously reported that abacavir is an inhibitor but not a substrate of the ENTs, with entry into HeLa cells limited to diffusion (Miller et al., 2020). The IC₅₀ values determined in the present study for abacavir against ENT1- and ENT2-mediated [³H]uridine

uptake showed that abacavir has ~3.7-fold higher affinity for ENT1 than ENT2.

We expanded our investigation into ENT-drug interactions by testing 37 nucleoside/heterocycle analogs. These compounds are structurally diverse and range in molecular weight from 225 to 735 g/mol. Seventeen compounds inhibited uptake in at least one of the cell lines: GS-9667, lexibulin, ticagrelor,

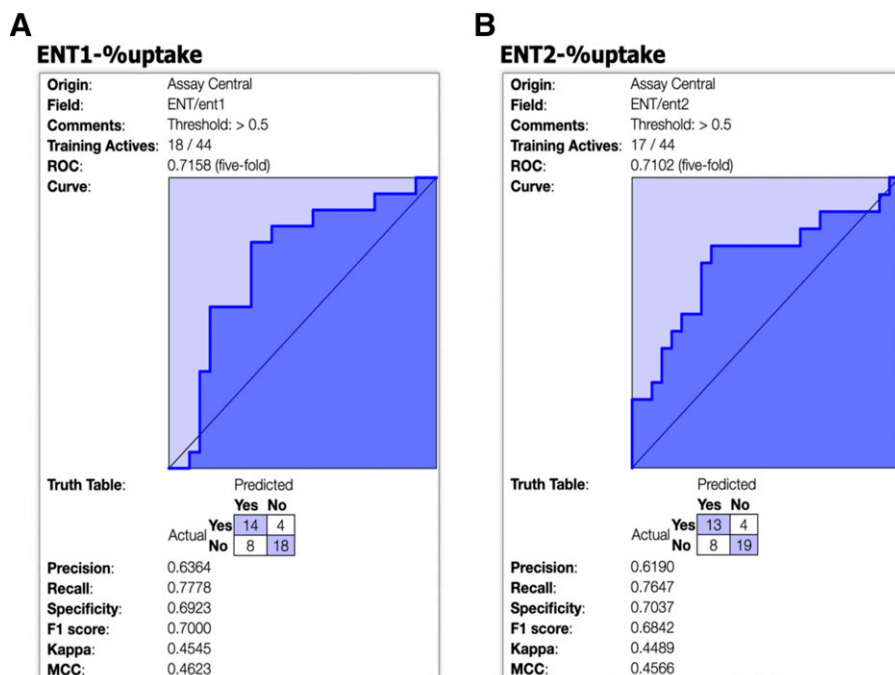


Fig. 10. ROC graphs generated from Assay Central machine learning models for ENT1 and ENT2. The x-axis is the false positive rate, and the y-axis is the true positive rate. Bayesian models for ENT1 (A) and ENT2 (B). Models were created using the nucleoside/heterocycle analogs in Fig. 7 and endogenous nucleosides. Predictions were evaluated using a standard probability cutoff at 0.5, wherein a value greater than 0.5 was considered active. Compounds were further classified as active if the inhibition of uridine uptake was greater than 50%. Truth tables showing the number of false positive, false negative, true positive, and true negative inhibitors are included. Other statistical parameters including precision, recall, specificity, F1 score, κ , and MCC are defined.

GS-6620, darusentan, acalisib, GS-0938, GS-9191 uridine triacetate, clofarabine, cladribine, darunavir, nelarabine, nevirapine, eleclazine, mercitabine, and tecadenoson. Of the nucleoside/heterocycle analogs that inhibited uptake, 76% had a molecular weight over 300 g/mol. Of the nucleoside/heterocycle analogs that failed to inhibit uptake, 65% had a molecular weight below 300 g/mol. Based on this limited data set, it appears that inhibition of ENT activity correlates with increased

molecular weight. GS-9667 was the most potent inhibitor of ENT1 (estimated $IC_{50} = \sim 4 \mu\text{M}$), whereas GS-6620 was the most potent inhibitor of ENT2 (estimated $IC_{50} = \sim 14 \mu\text{M}$). The large difference in affinity of ENT1 and ENT2 for NBMPR shows that these two homologous transporters (amino acid sequence identity of $\sim 45\%$) have markedly different selectivity profiles. Here, we found that three compounds, nevirapine, ticagrelor, and uridine triacetate, had different inhibitory profiles for ENT1 and ENT2. Nevirapine

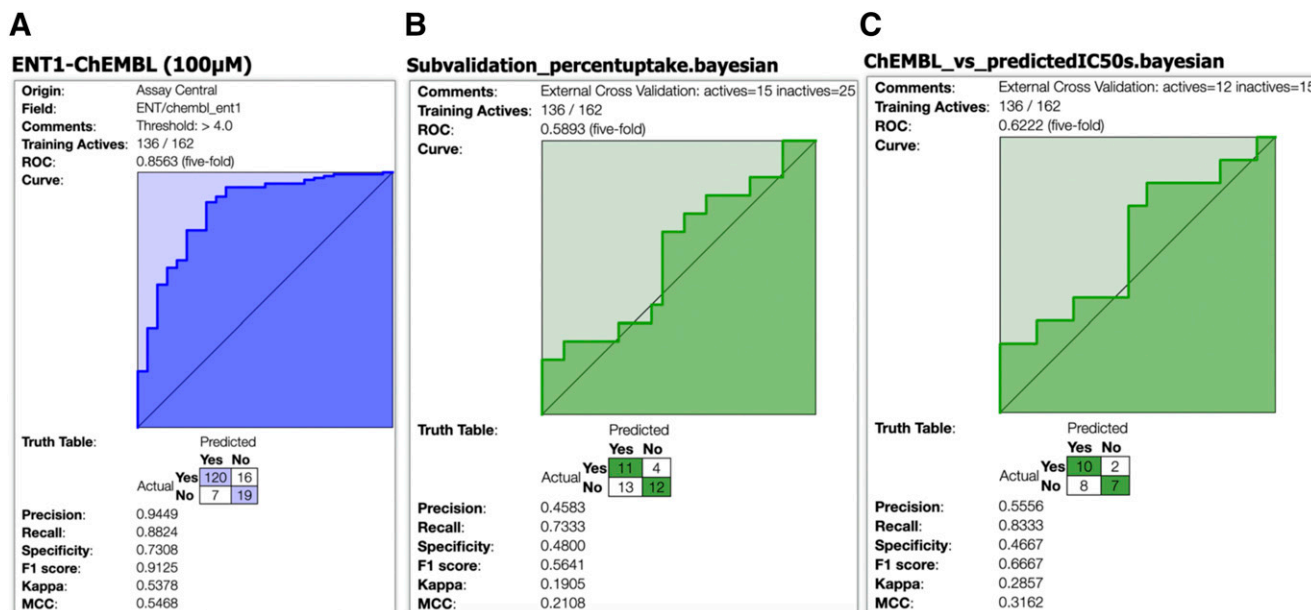


Fig. 11. ROC graphs generated from Assay Central machine learning models for ENT1 using the ChEMBL data set. The x-axis is the false positive rate, and the y-axis is the true positive rate. The ENT1 training model (A) was built from all IC_{50} data available from ChEMBL Target ID 1997 (https://www.ebi.ac.uk/chembl/target_report_card/CHEMBL1997/), and the threshold was set at 100 μM . The percent uptake subvalidation (B) test was defined by binary classification of percent uptake <50% with 40 compounds total. The estimated- IC_{50} values subvalidation (C) test was defined by binary classification of estimated- IC_{50} values of less than 100 μM with 27 compounds total. Truth tables showing the number of false positive, false negative, true positive, and true negative inhibitors are included. Other statistical parameters including precision, recall, specificity, F1 score, κ , and MCC are defined.

more potently inhibited ENT2 than ENT1, and ticagrelor and uridine triacetate were more potent inhibitors of ENT1 than ENT2 (Fig. 7 and Fig. 8B).

The ENTs are not included by the International Transporter Consortium (Giacomini et al., 2010), the US Food and Drug Administration (United States Department of Health and Human Services, 2017), or the European Medicines Agency (European Medicines Agency Committee for Human Medicinal Products, 2012) as transporter targets for unwanted DDIs. Nevertheless, their recommendation that unbound C_{\max}/IC_{50} ratios of ≥ 0.1 as indicators of potential unwanted DDIs suggests that interactions of ENT1 with abacavir [IC_{50} value of 85.7 μM and C_{\max} of 2.23–15.3 μM (Hervey and Perry, 2000)] produce a C_{\max}/IC_{50} of 0.026–0.179, suggesting it could contribute to unwanted inhibition of transport of endogenous nucleosides.

The initial screening of the nucleoside/heterocycle analogs only identifies interactions and does not determine whether these compounds are substrates or inhibitors of the ENTs. The classification of identified inhibitors of the ENTs was explored for nevirapine, lexibulin, clofarabine, and cladribine. Transport of these compounds with and without 100 μM NBMPR was measured and detected by LC-MS/MS. Compounds without a decrease in uptake in the presence of NBMPR were concluded to be inhibitors at the tested concentration. Compounds with a decrease in uptake in the presence of NBMPR were classified as substrates. A decrease in clofarabine and cladribine uptake in the presence of NBMPR suggests both compounds are substrates (and competitive inhibitors of uridine uptake) of both transporters. No change in nevirapine uptake in the presence of NBMPR suggests that nevirapine is a nontransported inhibitor of both ENT1 and ENT2. No change in lexibulin uptake in the presence of NBMPR in ENT1 cells was observed, suggesting it is a nontransported inhibitor of ENT1. An increase in uptake in ENT2 cells in the presence of NBMPR suggests that lexibulin is also a nontransported inhibitor of ENT2. Further investigation into compounds that interact with the ENTs will classify compounds as substrates or inhibitors and may reveal differences in substrate selectivity between ENT1 and ENT2.

We identified significant interactions with both ENT1 and ENT2 for clofarabine and cladribine, as have previous studies (King et al., 2006). Gemcitabine is a widely accepted substrate of the ENTs (Hammond et al., 1999; Santini et al., 2011; Vincenzi et al., 2017; Hioki et al., 2018; Kim et al., 2018). Although gemcitabine is a substrate, we observed modest inhibition of [^3H]uridine uptake in the presence of gemcitabine, which was consistent with other reports of gemcitabine inhibition of [^3H]uridine uptake (Shimada et al., 2015; Hioki et al., 2018). Trifluridine is a reported substrate of both ENT1 and ENT2, and we observed modest interactions with ENT1 and ENT2 (Takahashi et al., 2018). Interestingly, cytarabine did not inhibit ENT1 activity and slightly inhibited ENT2 activity, although cytarabine is a substrate of both transporters (Wiley et al., 1983; White et al., 1987; Clarke et al., 2006; Català et al., 2016). Modest interactions with azacitadine and ENT1 and with decitabine and ENT2 were identified, although previous studies report both compounds as substrates for both transporters (Damaraju

et al., 2012; Hummel-Eisenbeiss et al., 2013; Arimany-Nardi et al., 2014).

Bayesian machine learning models have been successfully and widely used to predict chemical bioactivity and improve and facilitate the drug discovery process. Using the Assay Central software, we generated predictive Bayesian models for inhibitors of ENT1 and ENT2 (Lane et al., 2018; Russo et al., 2018; Zorn et al., 2019). These models of ENT1 and ENT2 inhibition performed well in 5-fold crossvalidation as demonstrated by internal ROC scores greater than 0.7. Subvalidations based on the ENT1 training model built from IC_{50} data available from ChEMBL show that the model successfully predicted the majority of compounds that interact with ENT1. Using percent uptake, 58% of the inhibitors were correctly identified, and using estimated- IC_{50} values, 63% of the inhibitors were correctly identified. Testing additional diverse compounds and generating true IC_{50} values for identified inhibitors of ENT1 and ENT2 will aid in improving the Bayesian models as tools for increasing the efficiency of drug development as well as contributing to the generation of quantitative pharmacophores for these transporters.

In conclusion, the CRISPR/Cas9 system was used to produce HeLa cell lines that functionally expressed either ENT1 or ENT2, which were used to evaluate the impact of therapeutically relevant nucleoside-based compounds on transporter function. Moreover, these cell lines were crucial for the generation of predictive models for drug interactions with ENT1 and ENT2. There were marked differences in ENT1 and ENT2 selectivity with abacavir, nevirapine, ticagrelor, and uridine triacetate. Machine learning models based on these results can predict probable inhibitory interactions with the ENTs. Additionally, determining the structural differences in substrates for both transporters is essential in order to develop BTB-permeable compounds using the ENT1-ENT2 transepithelial transport pathway. Focused drug design informed by machine learning models developed from substrate selectivity data has the potential to improve the disposition of drugs by ENTs to treat viral infections and cancer in the MGT.

Acknowledgments

We thank Gilead Sciences Inc. (Foster City, CA) for providing us with selected compounds and Bill Smith for advice and review of the manuscript. We also thank Alex M. Clark (Molecular Materials Informatics, Inc.) for Assay Central support.

Authorship Contributions

Participated in research design: Miller, Jilek, Jennings, Galligan, Foil, Zorn, Ekins, Wright, Cherrington.

Conducted experiments: Miller, Zhang, Hau, Jilek, Jennings, Foil, Zorn, Ekins.

Performed data analysis: Miller, Zhang, Hau, Jilek, Jennings, Foil, Zorn, Ekins, Wright.

Wrote or contributed to the writing of the manuscript: Miller, Zhang, Hau, Jilek, Jennings, Galligan, Foil, Zorn, Ekins, Wright, Cherrington.

References

- Arimany-Nardi C, Errasti-Murugarren E, Minuesa G, Martínez-Picado J, Gorboulev V, Koepsell H, and Pastor-Anglada M (2014) Nucleoside transporters and human organic cation transporter 1 determine the cellular handling of DNA-methyltransferase inhibitors. *Br J Pharmacol* **171**:3868–3880.
- Boleti H, Coe IR, Baldwin SA, Young JD, and Cass CE (1997) Molecular identification of the equilibrative NBMPR-sensitive (es) nucleoside transporter and demonstration of an equilibrative NBMPR-insensitive (ei) transport activity in human erythroleukemia (K562) cells. *Neuropharmacology* **36**:1167–1179.

- Boswell-Casteel RC and Hays FA (2017) Equilibrative nucleoside transporters-A review. *Nucleosides Nucleotides Nucleic Acids* **36**:7–30.
- Cardona Maya WD, Du Plessis SS, and Velilla PA (2020) SARS-CoV-2 and the testis: similarity with other viruses and routes of infection. *Reprod Biomed Online* **40**: 763–764.
- Carletta J (1996) Assessing agreement on classification tasks: the kappa statistic. *Comput Linguist* **22**:249–254.
- Catalá A, Pastor-Anglada M, Caviedes-Cárdenas L, Malatesta R, Rives S, Vega-García N, Camós M, and Fernández-Calotti P (2016) FLT3 is implicated in cytarabine transport by human equilibrative nucleoside transporter 1 in pediatric acute leukemia. *Oncotarget* **7**:49786–49799.
- Clark AM, Dole K, Coulon-Spektor A, McNutt A, Grass G, Freundlich JS, Reynolds RC, and Ekins S (2015) Open source bayesian models. 1. Application to ADME/tox and drug discovery datasets. *J Chem Inf Model* **55**:1231–1245.
- Clark AM and Ekins S (2015) Open source bayesian models. 2. Mining a “big dataset” to create and validate models with ChEMBL. *J Chem Inf Model* **55**: 1246–1260.
- Clarke ML, Damaraju VL, Zhang J, Mowles D, Tackaberry T, Lang T, Smith KM, Young JD, Tomkinson B, and Cass CE (2006) The role of human nucleoside transporters in cellular uptake of 4'-thio- β -D-arabinofuranosylcytosine and β -D-arabinosylcytosine. *Mol Pharmacol* **70**:303–310.
- Cohen J (1960) A coefficient of agreement for nominal scales. *Psychol Meas* **20**:37–46.
- Cong L and Zhang F (2015) Genome engineering using CRISPR-Cas9 system. *Methods Mol Biol* **1239**:197–217.
- Dahlig-Harley E, Eilam Y, Paterson ARP, and Cass CE (1981) Binding of nitrobenzylthioinosine to high-affinity sites on the nucleoside-transport mechanism of HeLa cells. *Biochem J* **200**:295–305.
- Damaraju VL, Mowles D, Yao S, Ng A, Young JD, Cass CE, and Tong Z (2012) Role of human nucleoside transporters in the uptake and cytotoxicity of azacitidine and decitabine. *Nucleosides Nucleotides Nucleic Acids* **31**:236–255.
- Durmus S, Hendriks JJMA, and Schinkel AH (2015) Apical ABC transporters and cancer chemotherapeutic drug disposition. *Adv Cancer Res* **125**:1–41.
- Eastman RT, Roth JS, Brimacombe KR, Simeonov A, Shen M, Patnaik S, and Hall MD (2020) Remdesivir: a review of its discovery and development leading to emergency use authorization for treatment of COVID-19. *ACS Cent Sci* **5**:672–683.
- European Medicines Agency Committee for Human Medicinal Products (2012) Guideline on the investigation of drug interactions. https://www.ema.europa.eu/en/documents/scientific-guideline/guideline-investigation-drug-interactions-revision-1_en.pdf.
- Ewald B, Sampath D, and Plunkett W (2008) Nucleoside analogs: molecular mechanisms signaling cell death. *Oncogene* **27**:6522–6537.
- Gaffney DO, Jennings EQ, Anderson CC, Marentette JO, Shi T, Schou Oxvig A-M, Streeter MD, Johannsen M, Spiegel DA, Chapman E, et al. (2020) Non-enzymatic lysine lactoylation of glycolytic enzymes. *Cell Chem Biol* **27**: 206–213.e6.
- Griffith DA and Jarvis SM (1996) Nucleoside and nucleobase transport systems of mammalian cells. *Biochim Biophys Acta* **1286**:153–181.
- Hammond JR, Lee S, and Ferguson PJ (1999) [3H]gemcitabine uptake by nucleoside transporters in a human head and neck squamous carcinoma cell line. *J Pharmacol Exp Ther* **288**:1185–1191.
- Hervey PS and Perry CM (2000) Abacavir: a review of its clinical potential in patients with HIV infection. *Drugs* **60**:447–479.
- Hioki M, Shimada T, Yuan T, Nakanishi T, Tajima H, Yamazaki M, Yokono R, Takabayashi M, Sawamoto K, Akashita G, et al. (2018) Contribution of equilibrative nucleoside transporters 1 and 2 to gemcitabine uptake in pancreatic cancer cells. *Biopharm Drug Dispos* **39**:256–264.
- Huber-Ruano I and Pastor-Anglada M (2009) Transport of nucleoside analogs across the plasma membrane: a clue to understanding drug-induced cytotoxicity. *Curr Drug Metab* **10**:347–358.
- Hummel-Eisenbeiss J, Hascher A, Hals P-A, Sandvold ML, Müller-Tidow C, Lyko F, and Rius M (2013) The role of human equilibrative nucleoside transporter 1 on the cellular transport of the DNA methyltransferase inhibitors 5-azacytidine and CP-4200 in human leukemia cells. *Mol Pharmacol* **84**:438–450.
- Giacomini KM, Huang SM, Tweedie DJ, Benet LZ, Brouwer KL, Chu X, Dahlin A, Evers R, Fischer V, Hillgren KM, et al.; International Transporter Consortium (2010) Membrane transporters in drug development. *Nat Rev Drug Discov* **9**:215–236.
- Jordan PC, Stevens SK, and Deval J (2018) Nucleosides for the treatment of respiratory RNA virus infections. *Antivir Chem Chemother* **26**:2040206618764483.
- Jordheim LP, Durantel D, Zoulim F, and Dumontet C (2013) Advances in the development of nucleoside and nucleotide analogues for cancer and viral diseases. *Nat Rev Drug Discov* **12**:447–464.
- Kato R, Maeda T, Akaike T, and Tamai I (2005) Nucleoside transport at the blood-testis barrier studied with primary-cultured sertoli cells. *J Pharmacol Exp Ther* **312**:601–608.
- Kido Y, Matsson P, and Giacomini KM (2011) Profiling of a prescription drug library for potential renal drug-drug interactions mediated by the organic cation transporter 2. *J Med Chem* **54**:4548–4558.
- Kim J, Kim H, Lee J-C, Kim JW, Paik WH, Lee SH, Hwang J-H, Ryu JK, and Kim Y-T (2018) Human equilibrative nucleoside transporter 1 (hENT1) expression as a predictive biomarker for gemcitabine chemotherapy in biliary tract cancer. *PLoS One* **13**:e0209104.
- King KM, Damaraju VL, Vickers MF, Yao SY, Lang T, Tackaberry TE, Mowles DA, Ng AML, Young JD, and Cass CE (2006) A comparison of the transportability, and its role in cytotoxicity, of clofarabine, cladribine, and fludarabine by recombinant human nucleoside transporters produced in three model expression systems. *Mol Pharmacol* **69**:346–353.
- Klein DM, Evans KK, Hardwick RN, Dantzer WH, Wright SH, and Cherrington NJ (2013) Basolateral uptake of nucleosides by Sertoli cells is mediated primarily by equilibrative nucleoside transporter 1. *J Pharmacol Exp Ther* **346**:121–129.
- Koczor CA, Torres RA, and Lewis W (2012) The role of transporters in the toxicity of nucleoside and nucleotide analogs. *Expert Opin Drug Metab Toxicol* **8**: 665–676.
- Lane T, Russo DP, Zorn KM, Clark AM, Korotcov A, Tkachenko V, Reynolds RC, Perryman AL, Freundlich JS, and Ekins S (2018) Comparing and validating machine learning models for *Mycobacterium tuberculosis* drug discovery. *Mol Pharm* **15**:4346–4360.
- Lauzon GJ and Paterson AR (1977) Binding of the nucleoside transport inhibitor nitrobenzylthioinosine to HeLa cells. *Mol Pharmacol* **13**:883–891.
- Le Tortorec A and Dejucq-Rainsford N (2010) HIV infection of the male genital tract - consequences for sexual transmission and reproduction. *Int J Androl* **33**, e98–e108.
- Li D, Jin M, Bao P, Zhao W, and Zhang S (2020) Clinical characteristics and results of semen tests among men with coronavirus disease 2019. *JAMA Netw Open* **3**: e208292.
- Livak KJ and Schmittgen TD (2001) Analysis of relative gene expression data using real-time quantitative PCR and the 2(- $\Delta \Delta C(T)$) Method. *Methods* **25**:402–408.
- Lucas S and Nelson AM (2015) HIV and the spectrum of human disease. *J Pathol* **235**:229–241.
- Mackey JR, Yao SYM, Smith KM, Karpinski E, Baldwin SA, Cass CE, and Young JD (1999) Gemcitabine transport in xenopus oocytes expressing recombinant plasma membrane mammalian nucleoside transporters. *J Natl Cancer Inst* **91**:1876–1881.
- Matthews BW (1975) Comparison of the predicted and observed secondary structure of T4 phage lysozyme. *Biochim Biophys Acta* **405**:442–451.
- Miller SR and Cherrington NJ (2018) Trans epithelial transport across the blood-testis barrier. *Reproduction* **156**:R187–R194.
- Miller SR, Hau RK, Jilek JL, Morales MN, Wright SH, and Cherrington NJ (2020) Nucleoside reverse transcriptase inhibitor interaction with human equilibrative nucleoside transporters 1 and 2. *Drug Metab Dispos* **48**:603–612.
- Mruk DD and Cheng CY (2015) The mammalian blood-testis barrier: its biology and regulation. *Endocr Rev* **36**:564–591.
- Mruk DD, Su L, and Cheng CY (2011) Emerging role for drug transporters at the blood-testis barrier. *Trends Pharmacol Sci* **32**:99–106.
- Pastor-Anglada M and Pérez-Torras S (2015) Nucleoside transporter proteins as biomarkers of drug responsiveness and drug targets. *Front Pharmacol* **6**:13.
- Plagemann PGW, Marz R, and Wohlhueter RM (1978) Uridine transport in novikoff rat hepatoma cells and other cell lines and its relationship to uridine phosphorylation and phosphorolysis. *J Cell Physiol* **97**:49–72.
- Plagemann PGW and Wohlhueter RM (1984) Nucleoside transport in cultured mammalian cells. Multiple forms with different sensitivity to inhibition by nitrobenzylthioinosine or hypoxanthine. *Biochim Biophys Acta* **773**:39–52.
- Ran FA, Hsu PD, Wright J, Agarwala V, Scott DA, and Zhang F (2013) Genome engineering using the CRISPR-Cas9 system. *Nat Protoc* **8**:2281–2308.
- Rehan S, Shahid S, Salminen TA, Jaakola V-P, and Paavilainen VO (2019) Current progress on equilibrative nucleoside transporter function and inhibitor design. *SLAS Discov* **24**:953–968.
- Rozen S and Skaletsky H (2000) Primer3 on the WWW for general users and for biologist programmers. *Methods Mol Biol* **132**:365–386.
- Russo DP, Zorn KM, Clark AM, Zhu H, and Ekins S (2018) Comparing multiple machine learning algorithms and metrics for estrogen receptor binding prediction. *Mol Pharm* **15**:4361–4370.
- Sandoval PJ, Zorn KM, Clark AM, Ekins S, and Wright SH (2018) Assessment of substrate-dependent ligand interactions at the Organic Cation Transporter OCT2 using six model substrates. *Mol Pharmacol* **94**:1057–1068.
- Santini D, Schiavon G, Vincenzi B, Cass CE, Vasile E, Manazza AD, Catalan V, Baldi GG, Lai R, Rizzo S, et al. (2011) Human equilibrative nucleoside transporter 1 (hENT1) levels predict response to gemcitabine in patients with biliary tract cancer (BTC). *Curr Cancer Drug Targets* **11**:123–129.
- Shimada T, Nakanishi T, Tajima H, Yamazaki M, Yokono R, Takabayashi M, Shimada T, Sawamoto K, Miyamoto K-I, Kitagawa H, et al. (2015) Saturable hepatic extraction of gemcitabine involves biphasic uptake mediated by nucleoside transporters equilibrative nucleoside transporter 1 and 2. *J Pharm Sci* **104**:3162–3169.
- Sundaram M, Yao SY, Ingram JC, Berry ZA, Abidi F, Cass CE, Baldwin SA, and Young JD (2001) Topology of a human equilibrative, nitrobenzylthioinosine (NBMPR)-sensitive nucleoside transporter (hENT1) implicated in the cellular uptake of adenosine and anti-cancer drugs. *J Biol Chem* **276**:45270–45275.
- Takahashi K, Yoshisue K, Chiba M, Nakanishi T, and Tamai I (2018) Contribution of equilibrative nucleoside transporter(s) to intestinal basolateral and apical transports of anticancer trifluridine. *Biopharm Drug Dispos* **39**:38–46.
- United States Department of Health and Human Services (2017) In vitro metabolism and transporter-mediated drug-drug interaction studies guidance for industry draft guidance. In, Food and Drug Administration Center for Drug Evaluation and Research. Research, ed. <https://www.fda.gov/regulatory-information/search-fda-guidance-documents/vitro-drug-interaction-studies-cytochrome-p450-enzyme-and-transporter-mediated-drug-interactions>
- Vincenzi B, Stacchiotti S, Collini P, Pantano F, Rabitti C, Perrone G, Iuliani M, Baldi A, Badalamenti G, Sanfilippo R, et al. (2017) Human equilibrative nucleoside transporter 1 gene expression is associated with gemcitabine efficacy in advanced leiomyosarcoma and angiosarcoma. *Br J Cancer* **117**:340–346.
- Ward JL, Sherali A, Mo ZP, and Tse CM (2000) Kinetic and pharmacological properties of cloned human equilibrative nucleoside transporters, ENT1 and ENT2, stably expressed in nucleoside transporter-deficient PK15 cells. Ent2 exhibits a low affinity for guanosine and cytidine but a high affinity for inosine. *J Biol Chem* **275**: 8375–8381.
- White JC, Rathmell JP, and Capizzi RL (1987) Membrane transport influences the rate of accumulation of cytosine arabinoside in human leukemia cells. *J Clin Invest* **79**:380–387.
- Wiley JS, Jones SP, and Sawyer WH (1983) Cytosine arabinoside transport by human leukaemic cells. *Eur J Cancer Clin Oncol* **19**:1067–1074.

- Yao SY, Ng AM, Sundaram M, Cass CE, Baldwin SA, and Young JD (2001) Transport of antiviral 3'-deoxy-nucleoside drugs by recombinant human and rat equilibrative, nitrobenzylthioinosine (NBMPR)-insensitive (ENT2) nucleoside transporter proteins produced in *Xenopus* oocytes. *Mol Membr Biol* **18**: 161–167.
- Zorn KM, Lane TR, Russo DP, Clark AM, Makarov V, and Ekins S (2019) Multiple machine learning comparisons of HIV cell-based and reverse transcriptase data sets. *Mol Pharm* **16**:1620–1632.

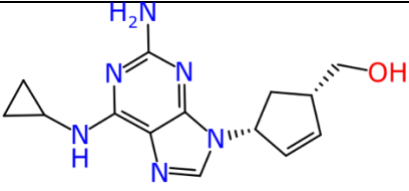
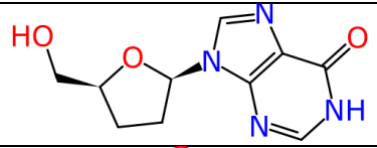
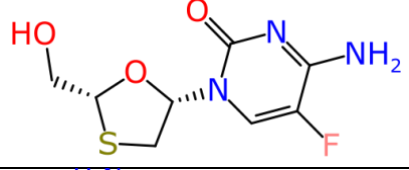
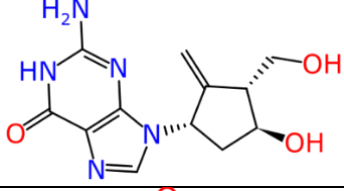
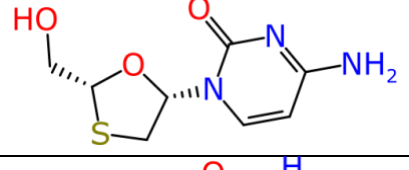
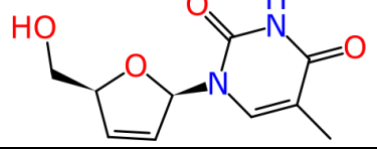
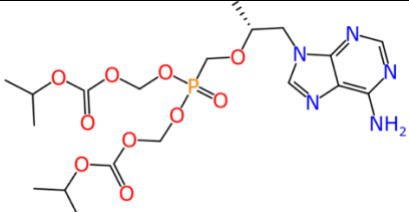
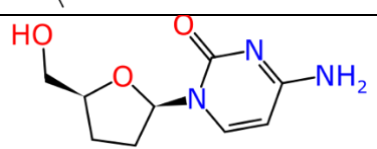
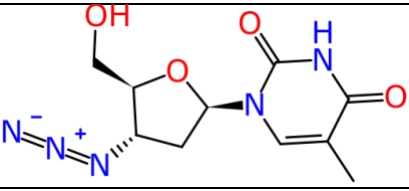
Address correspondence to: Nathan J. Cherrington, Department of Pharmacology and Toxicology, College of Pharmacy, University of Arizona, 1295 N Martin Ave., Tucson, AZ 85721. E-mail: cherring@pharmacy.arizona.edu; or Stephen H. Wright, Department of Physiology, College of Medicine, University of Arizona, 1501 N Campbell Ave., Tucson, AZ. 85724. E-mail: shwright@email.arizona.edu

MOLPHARM000169

Predicting Drug Interactions with Human Equilibrative Nucleoside Transporters 1 and 2 Using Functional Knockout Cell Lines and Bayesian Modeling

Siennah R. Miller, Xiaohong Zhang, Raymond K. Hau, Joseph L. Jilek, Erin Q. Jennings, James J. Galligan, Daniel H. Foil, Kimberley M. Zorn, Sean Ekins, Stephen H. Wright & Nathan J. Cherrington

Supplementary Table 1: Nucleoside Reverse Transcriptase Inhibitors (NRTIs). List of NRTIs with molecular weights and structures are listed for each NRTI.

<u>Structure</u>	<u>Name</u>	<u>MW (g/mol)</u>
	Abacavir	286.33
	Didanosine	236.23
	Emtricitabine	247.25
	Entecavir	277.28
	Lamivudine	229.26
	Stavudine	224.21
	Tenofovir Disoproxil	519.40
	Zalcitabine	211.22
	Zidovudine	267.24

MOLPHARM000169

Supplementary Table 2: List of compounds in the library provided by Gilead Sciences.

Compounds were provided as 10 mM stocks in DMSO. PubChem Identifiers (CID) and

URLs to the 2D structures are listed for each compound.

Analog	CID	PubChem Structure (URL)
Acalisib	11618268	https://pubchem.ncbi.nlm.nih.gov/compound/11618268#section=2D-Structure
Aciclovir	135398513	https://pubchem.ncbi.nlm.nih.gov/compound/135398513#section=2D-Structure
Azacitadine	9444	https://pubchem.ncbi.nlm.nih.gov/compound/9444#section=2D-Structure
Azathioprine	2265	https://pubchem.ncbi.nlm.nih.gov/compound/2265#section=2D-Structure
Capecitabine	60953	https://pubchem.ncbi.nlm.nih.gov/compound/60953#section=2D-Structure
Cidofovir	60613	https://pubchem.ncbi.nlm.nih.gov/compound/60613#section=2D-Structure
Cladribine	20279	https://pubchem.ncbi.nlm.nih.gov/compound/20279#section=2D-Structure
Clevudine	73115	https://pubchem.ncbi.nlm.nih.gov/compound/73115#section=2D-Structure
Clofarabine	119182	https://pubchem.ncbi.nlm.nih.gov/compound/119182#section=2D-Structure
Cytarabine	6253	https://pubchem.ncbi.nlm.nih.gov/compound/6253#section=2D-Structure
Darunavir	213039	https://pubchem.ncbi.nlm.nih.gov/compound/213039#section=2D-Structure
Darusentan	177236	https://pubchem.ncbi.nlm.nih.gov/compound/177236#section=2D-Structure
Decitabine	451668	https://pubchem.ncbi.nlm.nih.gov/compound/451668#section=2D-Structure
Dexelvucitabine	64973	https://pubchem.ncbi.nlm.nih.gov/compound/64973#section=2D-Structure
Doravirine	58460047	https://pubchem.ncbi.nlm.nih.gov/compound/58460047#section=2D-Structure
Eleclazine	71183216	https://pubchem.ncbi.nlm.nih.gov/compound/71183216#section=2D-Structure
Famciclovir	3324	https://pubchem.ncbi.nlm.nih.gov/compound/3324#section=2D-Structure
Fludarabine	657237	https://pubchem.ncbi.nlm.nih.gov/compound/657237#section=2D-Structure
Gemcitabine	60750	https://pubchem.ncbi.nlm.nih.gov/compound/60750#section=2D-Structure
GS-0938/PSI 938	46863668	https://pubchem.ncbi.nlm.nih.gov/compound/46863668#section=2D-Structure

GS-6201	11270783	https://pubchem.ncbi.nlm.nih.gov/compound/11270783#section=2D-Structure
GS-6620	58059494	https://pubchem.ncbi.nlm.nih.gov/compound/58059494#section=2D-Structure
GS-9191	44181731	https://pubchem.ncbi.nlm.nih.gov/compound/44181731#section=2D-Structure
GS-9667	11561692	https://pubchem.ncbi.nlm.nih.gov/compound/11561692#section=2D-Structure
Lexibulin	11351021	https://pubchem.ncbi.nlm.nih.gov/compound/11351021#section=2D-Structure
Mericitabine	16122663	https://pubchem.ncbi.nlm.nih.gov/compound/16122663#section=2D-Structure
Mizoribine	104762	https://pubchem.ncbi.nlm.nih.gov/compound/104762#section=2D-Structure
Nelarabine	3011155	https://pubchem.ncbi.nlm.nih.gov/compound/3011155#section=2D-Structure
Nevirapine	4463	https://pubchem.ncbi.nlm.nih.gov/compound/4463#section=2D-Structure
Presatovir	58029842	https://pubchem.ncbi.nlm.nih.gov/compound/58029842#section=2D-Structure
Rabacfosadine	16047979	https://pubchem.ncbi.nlm.nih.gov/compound/16047979#section=2D-Structure
Ribavirin	37542	https://pubchem.ncbi.nlm.nih.gov/compound/37542#section=2D-Structure
Tecadenoson	158795	https://pubchem.ncbi.nlm.nih.gov/compound/158795#section=2D-Structure
Telbivudine	159269	https://pubchem.ncbi.nlm.nih.gov/compound/159269#section=2D-Structure
Ticagrelor	9871419	https://pubchem.ncbi.nlm.nih.gov/compound/9871419#section=2D-Structure
Trifluridine	6256	https://pubchem.ncbi.nlm.nih.gov/compound/6256#section=2D-Structure
Uridine Triacetate	20058	https://pubchem.ncbi.nlm.nih.gov/compound/20058#section=2D-Structure

Supplementary Table 3: MRM transitions and calibration ranges for compounds used.

Abacavir served as an internal standard (IS) for nevirapine and lexibulin quantification, cladribine served as an IS for clofarabine quantification, and clofarabine served as an IS for cladribine quantification. DP, declustering potential; CE, collision energy. Entrance potential and collision cell exit potentials were both 10 V for all analytes.

Analyte	Parent Ion (Da)	Product Ion (Da)		Range (ng/mL)	R ²	DP (V)	CE (eV)
Clofarabine	304.1	170.1 (Quantifier)		5-100	0.9963	50	28
		134.1 (Qualifier)				50	55
Cladribine	286.0	170.0 (Quantifier)		5-100	0.9968	30	25
		117.1 (Qualifier)				40	25
Nevirapine	267.2	226.1 (Quantifier)		5-50	0.9914	90	15
		230.9 (Qualifier)				80	35
Lexibulin	435.4	257.0 (Quantifier)		10-100	0.9834	65	33
		360.2 (Qualifier)				65	40
Abacavir	287.1	150.0 (IS)				80	40

MOLPHARM000169

Supplemental File 1: Bayesian Modeling Output.

Prediction scores, applicability scores, percent uptake data, predicted and actual IC50 data is included. The green box indicates the compound was predicted to interact with ENT1 based on the Bayesian model generated from the ChEMBL dataset. Red indicates it was not predicted to interact with ENT1, and yellow indicates a potential interaction (close to the 0.5 cutoff for prediction score).

Name	ENT1 - ChEMBL - Threshold 100µM		Internal data							
	Prediction	Applicability	avg%uptake_ENT1	active_ENT1	avg%uptake_ENT2	active_ENT2	edictedIC50_ENT1_uM	edictedIC50_ENT2_uM	IC50_ENT1_uM	IC50_ENT2_uM
Acalisib	0.5464	0.3659	0.11939	1	0.093528654	1	27.11	20.63		
Aciclovir	0.3941	0.4510	0.863315	0	0.767707663	0	1263	661		
Adenosine	0.2045	In model	0.492505	1	0.286220219	1	194.1	80.2	39.92	56.55
Azacitadine	0.5076	0.7174	0.823231	0	0.955086929	0	931.4	4253		
Azathioprine	-0.4164	0.6545	1.039642	0	0.763361236	0		645.2		
Capecitabine	0.6644	0.6232	0.713873	0	0.748390212	0	499	594.9		
Cidofovir	0.3728	0.3878	1.11094	0	0.947359948	0		3599		
Ciadriline	0.6219	0.7895	0.24851	1	0.151481005	1	66.14	35.7		
Clevudine	0.5651	0.4600	1.026723	0	0.830972312	0		1465		
Clofarabine	0.5085	0.6379	0.174278	1	0.212813909	1	42.21	54.07		
Cytarabine	0.3521	0.7174	1.084683	0	0.722311655	0		520.2		
Cytidine	0.3307	0.7174	0.11328	1	0.717482292	0	25.55	507.9	21.08	368.2
Darunavir	0.5480	0.3804	0.255843	1	0.073245332	1	68.76	15.81		
Darusentan	0.6926	0.4706	0.09034	1	0.217160335	1	19.86	55.48		
Decitabine	0.6275	0.7292	1.047812	0	0.754185448	0		613.6		
Dexelvucitabine	0.4944	0.4167	1.330843	0	1.135705087	0				
Doravirine	0.4229	0.4267	1.135591	0	0.975853187	0		8083		
Eleclazine	0.6977	0.4384	0.509334	0	0.526722473	0	207.6	222.6		
Famciclovir	0.4365	0.5172	0.746415	0	0.726175145	0	588.7	530.4		
Fludarabine	0.5040	0.8000	1.037616	0	0.883612363	0		1518		
Gemcitabine	0.3707	0.5000	0.801583	0	0.614133934	0	808	318.3		
GS-0938	0.3740	0.4706	0.122672	1	0.071313587	1	27.96	15.36		
GS-452269	0.4095	0.3976	1.104376	0	0.986477785	0				
GS-465346	0.5221	0.3009	0.059823	1	0.066484224	1	12.72	14.24		
GS-9191	0.3311	0.5361	0.474267	1	0.661622666	0	180.4	391.1		
GS-9667	0.9146	0.8276	0.021066	1	0.107050869	1	4.303	23.98		
Guanosine	0.4775	0.6140	0.763838	0	0.805859627	0	646	830	385.9	254.9
Inosine	0.5877	0.5741	0.66328	0	0.333306504	1	394	99.99	219.5	27.02
Lexibulin	0.7533	0.4368	0.056681	1	0.150032196	1	12.02	35.3		
Mericitabine	0.2985	0.4203	0.511918	0	0.28090792	1	209.8	78.13		
Mizoribine	0.6342	0.7021	1.13182	0	0.991790084	0				
Nelarabine	0.4528	0.8793	0.482309	1	0.52962009	0	186.3	225.2		
Nevirapine	0.5738	0.4259	0.497812	1	0.106084997	1	198.3	23.73		
Presatovir	0.6189	0.3402	0.564572	0	0.698164842	0	259.3	462.6		
Rabacfosadine	0.2729	0.5432	1.038175	0	0.848358017	0		1119		

MOLPHARM000169

Ribavirin	0.6222	0.5870	1.006401	0	0.80537669	0		827.6		
Tecadenoson	0.7321	In model	0.551443	0	0.462009015	1	245.9	171.8		
Telbivudine	0.5785	0.4898	1.113105	0	0.774951706	0		688.7		
Thymidine	0.6553	0.7143	0.757414	0	0.386429491	1	624	126	708.9	138.1
Ticagrelor	0.7933	0.3535	0.058287	1	0.688023181	0	12.38	441.1		
Tracer+100uM NBMPR	0.8904	In model	-0.007495	1	0.051352222	1			0.01381	1.85
Tracer+5mM Uridine	0.5339	In model	-2.61E-18	1	-1.80175E-18	1				
Trifluridine	0.7069	0.7115	0.875326	0	0.800064392	0	1404	800.3		
Uridine Triacetate	0.5028	0.6552	0.124209	1	0.53348358	0	28.36	228.7		

Name	ENT1 - Miller - Threshold <50%uptake		ENT2 - Miller - Threshold <50%uptake		avg%uptake_ENT1	active_ENT1	avg%uptake_ENT2	active_ENT2	edictedIC50_ENT1_u	edictedIC50_ENT2_u	IC50_ENT1_uM	IC50_ENT2_uM
	Prediction	Applicability	Prediction	Applicability								
Adenosine	0.5463	0.8679	1.2555	0.8679	0.492505	1	0.286220219	1	194.1	80.2	39.92	56.55
Cytidine	-1.0099	0.9783	-0.4131	0.9783	0.11328	1	0.717482292	0	25.55	507.9	21.08	368.2
Guanosine	-0.4379	0.8421	-0.5179	0.8421	0.763838	0	0.805859627	0	646	830	385.9	254.9
Inosine	-0.0598	0.7222	-0.0156	0.7222	0.66328	0	0.333306504	1	394	99.99	219.5	27.02
Thymidine	-0.4465	0.9592	-0.8471	0.9592	0.757414	0	0.386429491	1	624	126	708.9	138.1